

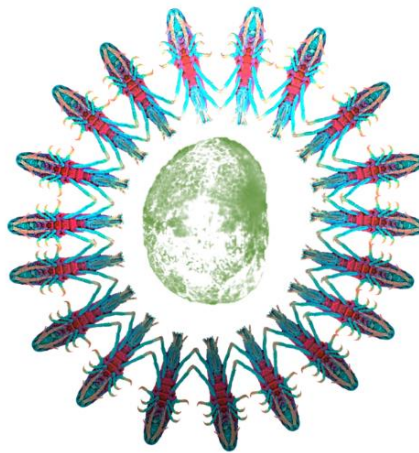
ΠΑΝΕΠΙΣΤΗΜΙΟ ΚΡΗΤΗΣ
ΣΧΟΛΗ ΘΕΤΙΚΩΝ ΚΑΙ ΤΕΧΝΟΛΟΓΙΚΩΝ ΕΠΙΣΤΗΜΩΝ
ΤΜΗΜΑ ΦΥΣΙΚΗΣ

ΔΙΠΛΩΜΑΤΙΚΗ ΕΡΓΑΣΙΑ

ΧΡΗΣΗ ΜΙΚΡΟΣΚΟΠΙΑΣ ΚΑΙ ΑΝΑΛΥΣΗΣ ΕΙΚΟΝΩΝ ΓΙΑ ΤΗΝ ΚΑΤΑΣΚΕΥΗ
ΑΝΑΠΤΥΞΙΑΚΩΝ ΚΥΤΤΑΡΙΚΩΝ ΓΕΝΕΑΛΟΓΙΩΝ

USE OF MICROSCOPY AND IMAGE ANALYSIS TOOLS FOR THE
RECONSTRUCTION OF DEVELOPMENTAL CELL LINEAGES

ΙΩΑΝΝΗΣ ΛΙΑΣΚΑΣ



Επιβλέπων: Αναστάσιος Παυλόπουλος
Εργαστήριο Ανάπτυξης και Μορφογένεσης
Ινστιτούτο Μοριακής Βιολογίας και Βιοτεχνολογίας
Ίδρυμα Τεχνολογίας και Έρευνας

Συνεπιβλέποντες: Γιάννης Ζαχαράκης
Δημήτριος Χαραλαμπίδης

ΗΡΑΚΛΕΙΟ, ΦΕΒΡΟΥΑΡΙΟΣ 2023

Acknowledgements:

There are many people that I would like to thank for their contribution to the present work. First and foremost Dr. Pavlopoulos who guided me throughout all of this work and was there to answer every question I had. I would like to thank all members of the Pavlopoulos lab, present and past, for their help, advice and friendship.

I would also like to thank the members of Dr Zacharakis's lab, as they were always supportive and eager to help me with the problems I faced. Special thanks go to Dr George Tserevelakis who taught me many technical aspects on microscopy and our collaboration resulted in my first publication.

My parents were, most of the times, a great support for finishing my exams and encouraging me to continue working hard in the lab.

I would also like to thank Ms Mary Kefalogianni for suggesting me to look for Dr Zacharakis's lab during my early years in Physics department.

Last but not least, I would like to thank the House of Craven for making the finest tobacco, important during the not so fine days.

INDEX:

0: Summary/Περίληψη	4
1: Introduction	5
1.1: Cell lineages in Developmental Biology	5
1.2: Fluorescent microscopy and fluorescent proteins	6
1.3: Computational tools for image analysis	7
1.4: The crustacean model organism <i>Parhyale hawaiiensis</i>	8
2: Materials and Methods	10
2.1: LSFM (Light-sheet Fluorescence Microscopy)	10
2.1.1: LSFM theory	10
2.1.2: Details on samples	12
2.1.3: Image Acquisition	12
2.1.4: Microscope parts and alignment	14
2.2: Image Processing	15
2.2.1: Interest Points	15
2.2.2: Registration and its success	15
2.2.3: Fusion	17
2.3: Lineage reconstruction	17
2.3.1: Mastodon	17
2.3.2: TGMM (Tracking with Gaussian Mixture Models)	17
2.3.3: The pipeline for producing the whole specimen	19
3: Results	19
3.1: LSFM (Light-sheet Fluorescence Microscopy)	19
3.1.1: LSFM images	19
3.2: Image Processing	22
3.2.1: Introduction	22
3.2.2: Multiview-Reconstruction	22
3.2.3: The results	22
3.2.4: Time Drift	22
3.2.5: Stitching	23
3.2.6: Deconvolution and Results	24
3.2.7: Keller pipeline	24
3.3: Lineage reconstruction	25
3.3.1: Introduction to lineage reconstruction	25
3.3.2: Datasets	25
3.3.3: The development of the embryo (a short introduction)	29
3.3.4: Migrations	29
3.3.5: The Grid	31
3.3.7: Neighborhood divisions	31
3.3.8: Population graphs and analysis	34
4: Discussion	36
5: Bibliography	38

0. SUMMARY/ΠΕΡΙΛΗΨΗ

A long-standing question in biology is how one cell, the fertilized egg, gives rise during embryogenesis to multiple cell types organized in tissue and organs of particular shape, size and function to suit the lifestyle of the whole organism. Recent advances in biology, physics and computer sciences allow to address these fundamental questions through the direct observation of all cells in live developing embryos and with the appropriate spatial and temporal resolution. My thesis focused on the first three days of development of the crustacean model organism *Parhyale hawaiiensis* to understand the cellular basis of ectoderm formation. Time-lapse image datasets of developing *Parhyale* embryos acquired by fluorescence light-sheet microscopy were first registered and fused computationally. Fluorescently labeled nuclei were segmented and tracked in these 4D volumes (3D+time) with a combination of automated tools and manual curation for the accurate and complete reconstruction of the embryonic cell lineages. These reconstructions have provided insights into the cellular behaviors shaping *Parhyale* embryos, including the number of constituent cells, the patterns of cell movement and the rules governing the contribution of distinct cell lineages to ectoderm formation. The tools and the knowledge gained from this study have paved the way for systems level analyses of developing embryos in the future.

Ένα από τα θεμελιώδη ερωτήματα στην βιολογία είναι πως ένα κύτταρο, το γονιμοποιημένο αυγό, δημιουργεί κατά τη διάρκεια της εμβρυογένεσης διαφορετικούς κυτταρικούς τύπους, που οργανώνονται σε ιστούς και όργανα με συγκεκριμένο σχήμα, μέγεθος και λειτουργία ώστε να υποστηρίζουν τη διαβίωση του οργανισμού. Πρόσφατες εξελίξεις στη βιολογία, τη φυσική και την επιστήμη υπολογιστών επιτρέπουν να απαντηθούν αυτές οι βασικές ερωτήσεις μέσω της άμεσης παρατήρησης των ζωντανών και αναπτυσσόμενων εμβρύων με την απαραίτητη χρονική και χωρική ευκρίνεια. Η εργασία μου επικεντρώνεται στις 3 πρώτες μέρες της ανάπτυξης του αναδυόμενου μοντέλου οργανισμού *Parhyale hawaiiensis* για την κατανόηση της κυτταρικής βάσης, του σχηματισμού του εκτοδέρματος. Time-lapse εικόνες αυτού του οργανισμού λήφθηκαν μέσω μικροσκοπίας φύλλου φωτός, ευθυγραμμίστηκαν και συγχωνεύθηκαν σε μία εικόνα 3 διαστάσεων μέσω υπολογιστικών τεχνικών. Οι φθορίζοντες πυρήνες εντοπίστηκαν και ιχνηλατήθηκαν στο χώρο και το χρόνο σε αυτά τα αρχεία 4 διαστάσεων (3D+χρόνος) χρησιμοποιώντας αυτόματα εργαλεία και ενδεδειγμένο έλεγχο για την δημιουργία ακριβών και πλήρων κυτταρικών γενεαλογιών. Μέσω αυτών των γενεαλογιών εξήχθησαν συμπεράσματα για τις κυτταρικές συμπεριφορές που σχηματίζουν τα έμβρυα του *Parhyale*. Σε αυτές συμπεριλαμβάνονται ο αριθμός των κυττάρων σε κάθε στάδιο της ανάπτυξης, τα πρότυπα κίνησης των κυττάρων και οι κανόνες που διέπουν τη συνεισφορά διαφορετικών κυτταρικών γενεαλογιών στο σχηματισμό του εκτοδέρματος. Τα εργαλεία και η γνώση που αποκτήθηκαν σε αυτή τη μελέτη ανοίγουν το δρόμο σε μελλοντικές, ολιστικές αναλύσεις της ανάπτυξης των εμβρύων.

1. Introduction:

1.1 Cell lineages in Developmental Biology

Even since 4th century B.C. it was observed that the offspring usually resembles its parents, picking several of their traits, so many concluded that this happens during embryogenesis and tried to explain how the development of an embryo works. Molecular biology and genetics were still unknown fields, so morphological and anatomical descriptions were the only ways to address the inner workings of developing embryos for centuries. Until the advent of molecular genetic labeling techniques, morphological studies relied on macroscopic and microscopic observations of transparent embryos that either had naturally pigmented cells or could be labeled with colored dyes to track cells (Buckingham and Meilhac, 2011; Kretzschmar and Watt, 2012).

Fate mapping studies in the early 20th century applied on invertebrate and vertebrate embryos, such as ascidians by Edwin Conklin and amphibians by Walter Vogt, started revealing what parts of the embryo and at what stage of development give rise to adult tissues and organs (mapping the fate of adult structures onto the embryo). The advance from coarse-grained fate maps to fine-grained fate maps with single cell resolution, called cell lineages, was made by John Sulston in the early 90s (Sulston *et al.*, 1983) (Figure 1.1 b). He was the first to track each and every cell and determine their divisions, movements and fates in embryos of the nematode *Caenorhabditis elegans*. *C. elegans* was the first organism to have its lineage completed, due to its simple and reproducible development, small cell number and its transparency. It was possible to observe it with just a differential interference contrast microscope and reconstruct the complete cell lineage by painstakingly collecting information from many embryos over several years.

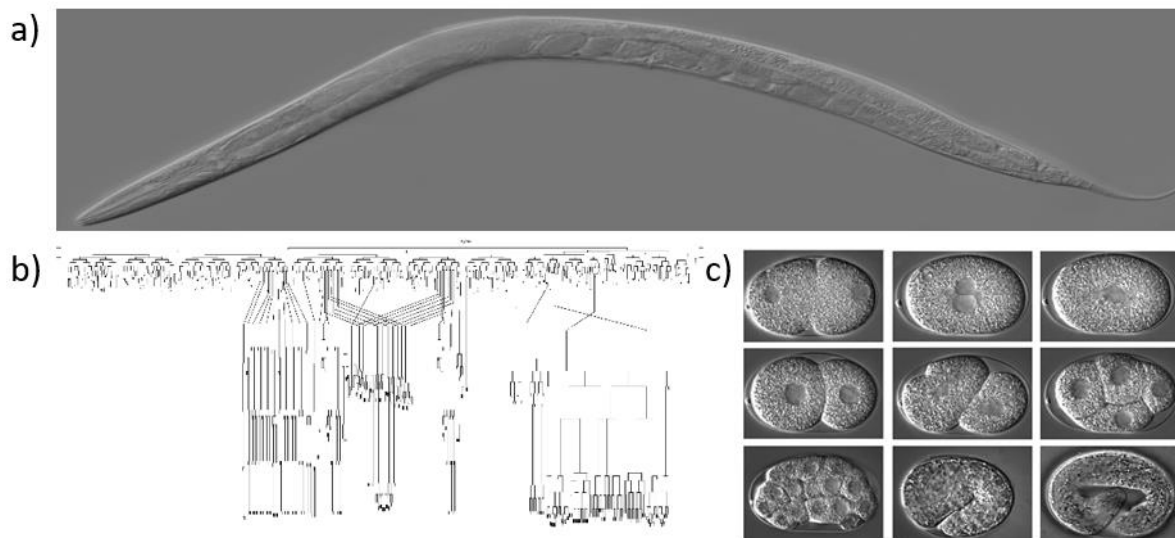


Figure 1.1: *C. elegans* and its complete cell lineage. a) The nematode *C. elegans*. b) The full cell lineage reconstruction of *C. elegans* embryogenesis (Sulston, 1983). c) Different stages of *C. elegans* embryogenesis under a differential interference contrast microscope. The circular shapes inside the cells are nuclei. Reproduced from (Sulston, 1983).

The work of Sulston, which granted him the Nobel Prize in Physiology or Medicine in 2002, was groundbreaking. It established *C. elegans* as a premier model for biological studies, where the development of each tissue could be analyzed at the single-cell level under wild-type and perturbed conditions. However, cell lineaging in more complex organisms, containing many more cells and developing over several days or weeks, is way more challenging. Several recent advances in microscopy techniques, genetic methods for fluorescence labeling and computational methods for image analysis are increasingly enabling scientists to reconstruct cell lineages in multicellular organisms. These methods are described below and were employed in my thesis to capture and analyze the behaviors of cells contributing to ectoderm formation in the genetically and optically tractable crustacean model *Parhyale hawaiiensis*.

1.2 Fluorescent microscopy and fluorescent proteins

The observation of embryos with light microscopes allows to see cells that are otherwise not visible by naked eye. There have been many advances since the usage of just two lenses and a light source (Compound Microscope, little is known about the first one, however one of the earliest was made by Zacharias Janssen and a great 3-D representation of such early microscopes is in <https://www.sciencemuseum.org.uk/objects-and-stories/medicine/microscope>) to observe the microscopic world. New phenomena like fluorescence (Köhler 1908 inefficient, Otto Heimstaedt 1911 and Heinrich 1913 efficient), photoacoustic, absorption, diffraction and others, helped researchers observe smaller and deeper structures, each giving us different information about biological specimens.

Fluorescence microscopy has become the most popular technique for biological applications because the structures of interest can be labelled genetically or chemically and imaged against a dark background. In particular, genetically encoded fluorescent proteins, such as the green fluorescent protein (GFP), can be excited by specific wavelengths and collect the emitted light in another specific wavelength. GFP was first identified in the jellyfish *Aequorea victoria* (Shimomura, 1979) and has been inserted into animals' genome (Figure 1.3). These genetically encoded fluorescent reporters were a huge leap for biology allowing to label every gene or subcellular structure of interest in a living organism and observe its structure and function. ((PDF) *Molecular Signalling Mechanisms at the μ -Opioid Receptor*, no date; Remington, 2011). The first fluorescence microscope was the widefield microscope using just a lamp, a filter and a dichroic mirror (Figure 1.2a). Taking it one step further, confocal scanning microscopy substituted the lamp with a laser, a scanning mirror and a pinhole for better optical sectioning, removing out-of-focus light and producing higher quality images with a better signal-to-noise ratio (Figure 1.2b). More recently, light-sheet fluorescence microscopy (LSFM) emerged as a better method for optical sectioning with faster acquisition rates, less photobleaching and phototoxicity, longer imaging sessions, from multiple angles (views) and a large selection of custom-built and commercial LSFM configurations. LSFM was used in this thesis for *Parhyale* imaging (Figure 1.2c) (VOIE, BURNS and SPELMAN, 1993; Huisken *et al.*, 2004; Santi, 2011; Stelzer, 2014; Wan, McDole and Keller, 2019; Stelzer *et al.*, 2021).

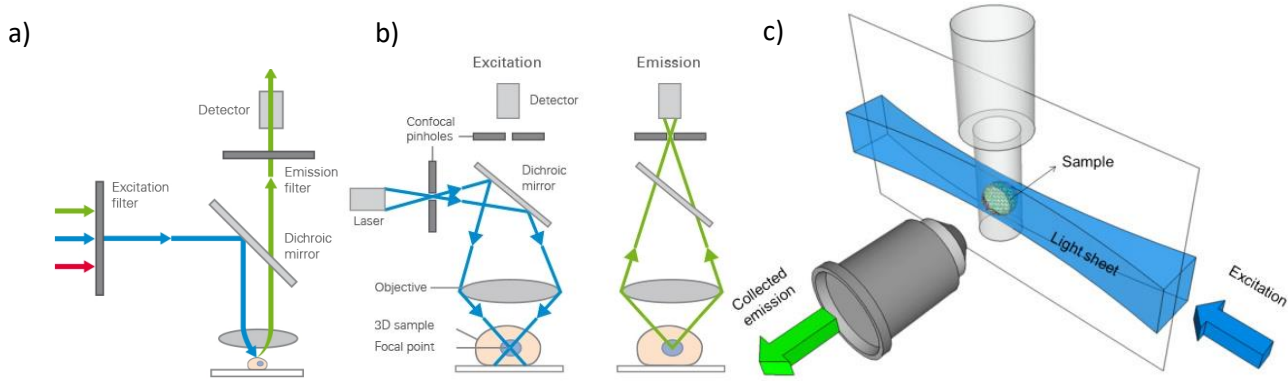


Figure 1.2. Schematics of the main fluorescence microscopy techniques. a) A simple schematic of a widefield microscope light pathway (*Widefield Fluorescence Microscopy | Principle & Applications | ibidi*, no date) b) Pathway of light in a confocal microscope; the main additions are the laser, the scanning mirror and the pinhole. (*Confocal Microscopy | Principle & Applications | ibidi*, no date) c) Simple schematic of the principle behind light sheet microscopes (Olarie *et al.*, 2018)

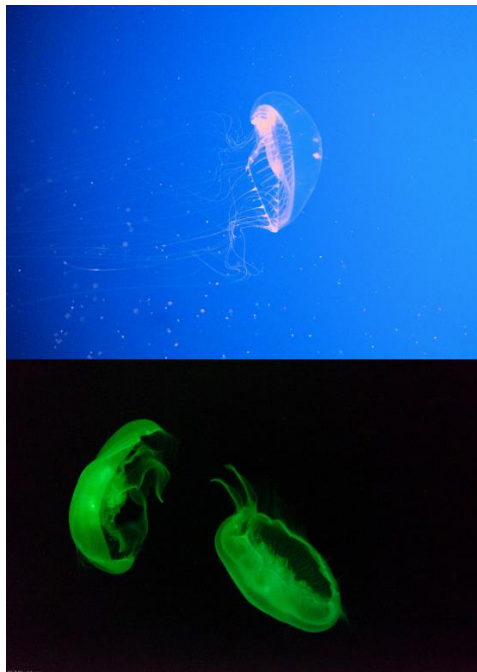


Figure 1.3. Fluorescent proteins and their origin. The jellyfish *Aequorea victoria* in the wild (top left), emitting fluorescence (bottom left), Jim G/Flickr (CC BY 2.0); Phil Blackburn/Flickr (CC BY-NC-ND 2.0), Structure of the Green Fluorescent Protein (bottom right).

1.3 Computational tools for image analysis

Another scientific domain important for microscopy is Computer Science for image processing. The images acquired from a microscope are processed in many different ways depending on the focus of the work. Advances in image processing are absolutely necessary for LSFM image datasets. In particular, multi-view LSFM, where series of optical sections (z-stacks) are acquired from multiple angles (views), requires the

alignment of these raw images in space (known as spatial registration) and their combination into a single output 3D image (known as spatial fusion) capturing the entire images volume. Furthermore, fused images can have an almost isotropic resolution through multi-view deconvolution. Last but not least, Artificial Intelligence based approaches can automate many image analysis steps, improving the accuracy and reducing the time required for manual curation. One of these tasks is the identification of cells in each 3D image (known as segmentation) and their observation over time in 4D (3D+time image datasets (known as tracking)).

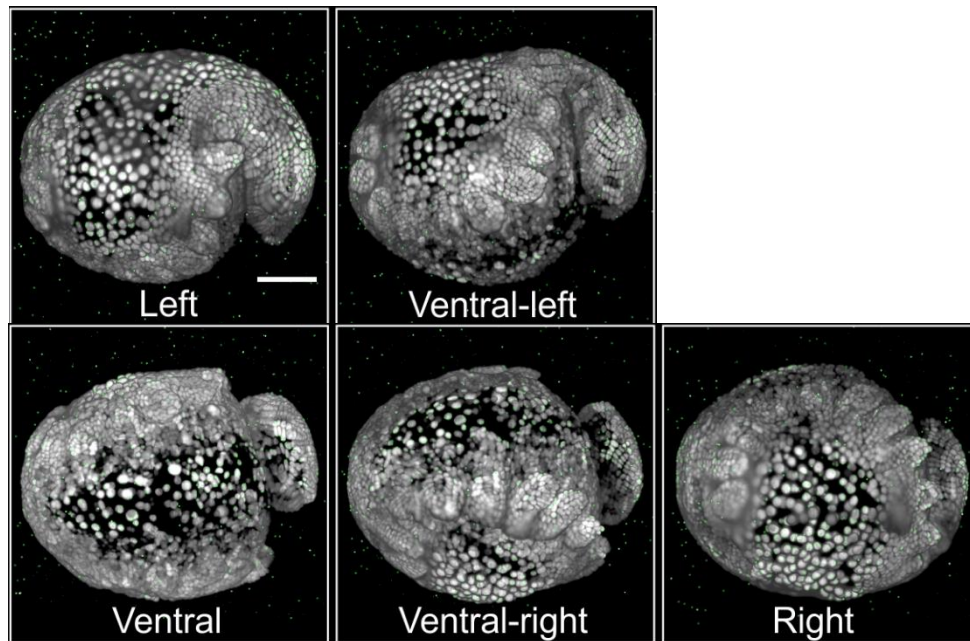


Figure 1.4. Raw multiview light-sheet imaging of a *Parhyale hawaiiensis* embryo. A transgenic *Parhyale hawaiiensis* embryo with H2B-mRFP labeled nuclei. This sample was imaged every 45° for each of the 5 indicated views. The green dots surrounding the embryos correspond to the scattered fluorescent beads used for image registration. Image reproduced from (Wolff et al. 2018).

1.4 The crustacean model organism *Parhyale hawaiiensis*

The amphipod crustacean *Parhyale hawaiiensis* used in this study is an emerging model organism. Emerging models complement existing model organisms used in laboratories, such as *Escherichia coli*, *Drosophila melanogaster*, *C. elegans*, zebrafish and mice, to provide new knowledge and understand the origin of diversity observed in nature (Sun and Patel, 2019). The advantages of this species are that their egg are optically and genetically tractable, making it possible to image in detail the whole embryo and manipulate it's genetic content (Konarakis and Pavlopoulos, 2014; Nast and Extavour, 2014). *Parhyale* is also a robust animal and a direct developer, which means that most adult body parts develop during the 10 days of embryogenesis and the hatchling is a miniature version of the adult. Also, recently has been shown that it can be a great model for regeneration (Konstantinides and Averof, 2014). Their embryogenesis begins with a total cleavage, when it reaches the 8-cell stage all cells have a different fate, 4 macromeres and 4

micromeres. The 4 macromeres are Ep (ectoderm posterior), El (ectoderm left), Er (ectoderm right) and Mav (mesoderm visceral), the 4 micromeres are en (endoderm), ml (mesoderm left), mr (mesoderm right) and g (germ line). 3 out of the 4 macromeres will make the ectoderm and organize and produce the grid, a highly organized structure special to only amphipods and the remaining will produce mesoderm and endoderm (Browne *et al.*, 2005; Alwes, Hinchin and Extavour, 2011).

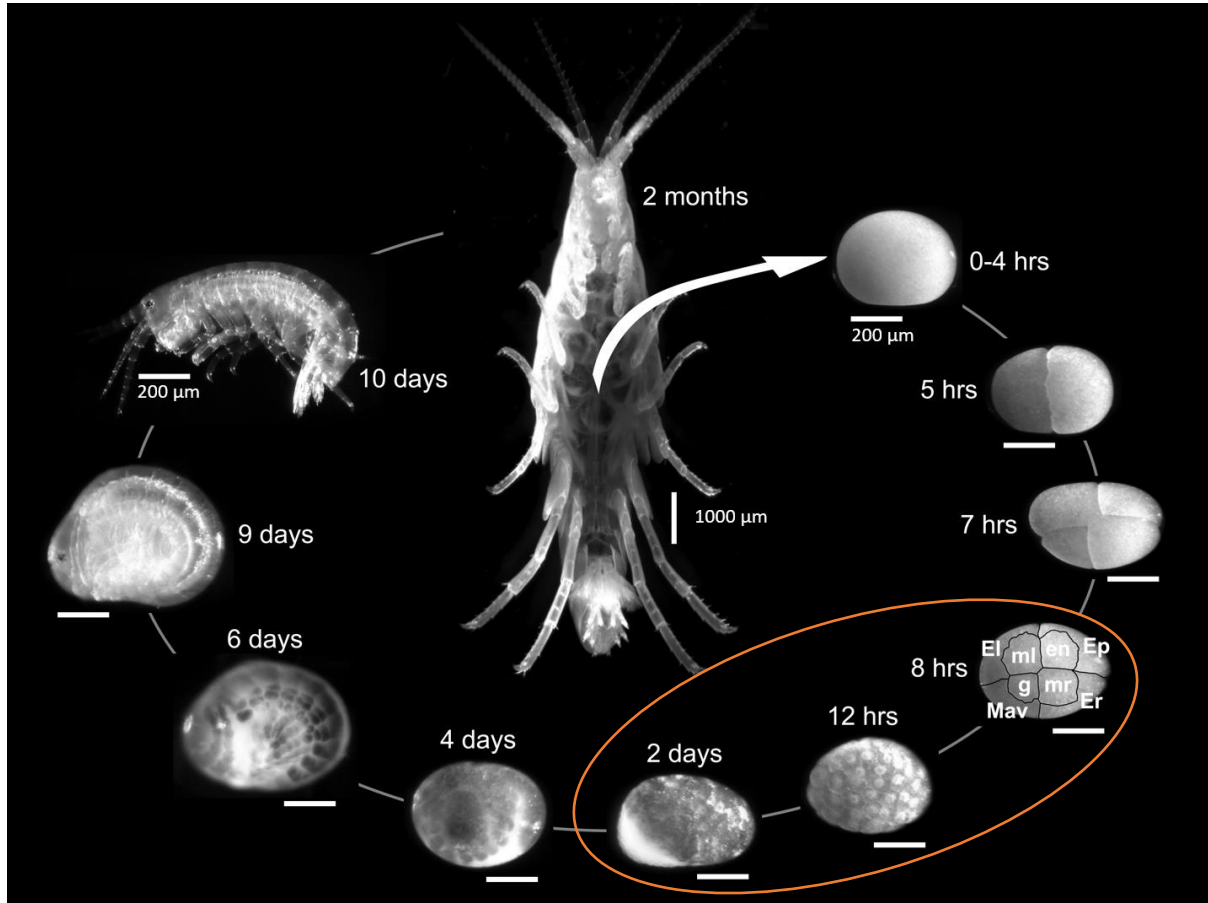


Figure 1.5. *Parhyale hawaiiensis* life cycle. Fertilized eggs are laid inside a pouch in the female and can be dissected to manipulate or image the embryos. The first cleavage stages show embryos at the 1-cell stage (0-4 hours), 2-cell stage (5 hours), 4-cell stage (7 hours) and 8-cell stage (8 hours) with 4 micromeres and 4 macromeres, each committed to a specific fate. This last stage is where our image datasets start and cover the following 2.5 days (indicated with orange cycle). Image reproduced from (Stamatakis and Pavlopoulos, 2016).

2. Materials and methods

2.1: LSFM (Light-sheet Fluorescence Microscopy):

2.1.1: LSFM theory

Fluorescence:

As previously described fluorescence is fundamental for biological microscopy, so it's important to show its inner workings.

The main principle is the one of the interactions between photons and electrons. The electron absorbs one photon (more in special scenarios) when they come in great proximity with each other. So the energy of the electron rises to be the sum of the energies of both particles, then the electron "loses energy" with non-radiative vibrational relaxations, until it reaches a specific energy level and then it will emit a new photon, and the electron will come back to its starting energy level. This new photon has a longer wavelength (less energy). It's a spherical phenomenon, which means the emitted wave has no relation with the incident angle. High laser intensity may produce photobleaching, so the fluorescent protein loses its fluorescence, making imaging impossible. So the intensity of the laser should be low enough to not damage the embryo or even the fluorescent proteins, but high enough to be able to illuminate the focused volume.

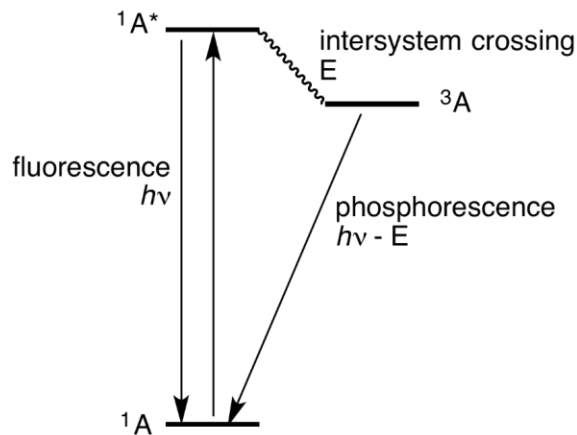


Figure 2.1. A Jablonski diagram. An electron absorbs light and is excited to $^1A^*$ state. Then there are 2 options, either emit light through fluorescence and reach the ground state (singlet state), or through intersystem crossing (non-emitting) reach a triplet state and then relax through phosphorescence (far less probable phenomenon not useful in microscopy). Image copied from https://en.wikipedia.org/wiki/Jablonski_diagram.

Optical sectioning:

To study the whole 3-D volume of a specimen there is a need for sectioning of the organism, making the axial resolution related to the thickness of each section. The first kind of sectioning was physical, by cutting

or ablating a section to continue to the next one, however this is fatal for biological specimens. Thus, a need for new non-fatal ways to produce sections has surfaced. The confocal microscope has shown that such non-fatal optical sections are possible, using focus rings and a pinhole to cut out the out of focus light or by illuminating and detecting only parts (sections) of the specimens. Great sectioning capabilities is a fundamental feature of light sheet microscopy. Images (a matrix with values or the sum of 3 matrices for RGB images) from optical sections produce stacks, an array of images (a tensor Figure 3.2) and voxel replaces the pixel of 2-D images, due to the need of depth definition, so there are 2 resolutions in a stack the axial and the lateral. Another technique SPIM excels at is Multiview imaging, imaging through many different angles. That way combining the different views one can produce an image with good axial and lateral resolution.



Figure 2.2. Image Quantization Matrix.
Representation of a digital image as a matrix of grayscale values.

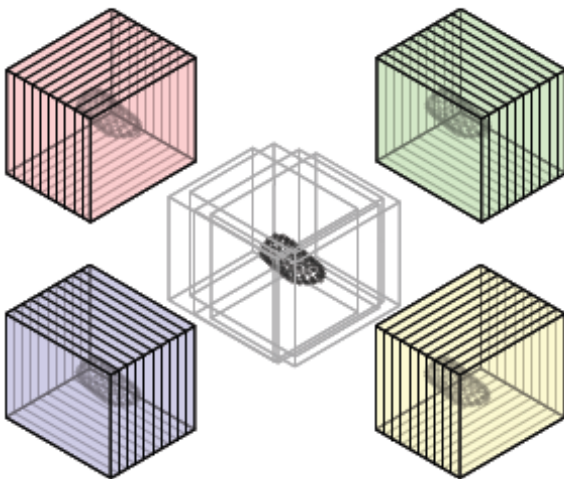


Figure 2.3. Schematics of Multiview Microscopy. Four z-stacks (views), 90° apart, are acquired, registered and fused into a single output z-stack containing the entire imaged volume with a more isotropic resolution. Image reproduced from (Preibisch *et al.*, 2010).

Light sheet theory:

Before going on to the rest of the materials and methods I think it is important to explain how the formation of light sheet works and show why low NA lenses are a requirement. I will not get into detail of how

mirrors, lenses and telescopes and work as they are trivial. Generally light sheet microscopes are built with Gaussian beams, there are works on other beams like Bessel and Airy (Vettenburg *et al.*, 2014; Meinert and Rohrbach, 2019), so the width of the Gaussian beam is defined by this equation:

$$w(z) = w_0 \sqrt{1 + \left(\frac{z}{z_R}\right)^2} \quad (1)$$

Where w_0 is the minimum width, z is the distance from the focal length and z_R (Rayleigh length) is defined as

$$z_R = \frac{\pi w_0^2}{\lambda} \quad (2)$$

Laser beams are rotationally symmetric, however light sheet beams are elongated on one axis, and this equation becomes important for the width of the light sheet and not its height.

Now I will show how the beam divergence relates to NA

$NA = n \sin(\theta)$ (3), $\theta = \frac{\lambda}{\pi w_0}$ (4), for very small angles $\sin(\theta) \sim \theta$, so (3) and (4) produce

$$w_0 = \frac{n\lambda}{\pi NA} \quad (5)$$

So a large w_0 is needed to have a large z_R to keep the light sheet stable, however a light sheet with large width is useless, so an equilibrium between the stability of the sheet and the sheet width should be found.

2.1.2: Details on samples:

Sample mounting:

For mounting, 1.5% low melting agarose gel (85% Artificial seawater (ASW): Dissolved sea salt in purified water (about 34 g/l) to a specific gravity of about 1.022) with beads FZ or FY (Etapor Microspheres), were fitted in a glass capillary with the sample, after the stabilization of this gel (5-10 minutes), the capillary was mounted on the SPIM chamber (Kontarakis and Pavlopoulos, 2014).

Gut Extraction:

For gut preparation, the specimen is anaesthetized through CO₂ and placed on a petri dish with gel, then with scissors its most part is cut. Holding its head with one tong and the rest of the body I would gently pull the head until the body would slide off, leaving the head with the whole digestive system intact, then I would crush and remove the head and the brain leaving only the esophagus.

2.1.3: Image Acquisition:

μManager:

All of the compartments of the microscope need a master handler to use them all in the right time, in this case the handler was μmanager (Edelstein *et al.*, 2014). This program can show a live image of the specimen, control the stage and the exposure of the camera. After setting the camera exposure and the laser intensity, it is time to acquire the images, using the Multi-Dimensional acquisition, I found all the positions I wanted to acquire, set the z length equal to ~70% of the specimen and acquired the image. There is the

possibility to change the acquisition order to get all channels for each slice or first all the slices for one channel and then the others.

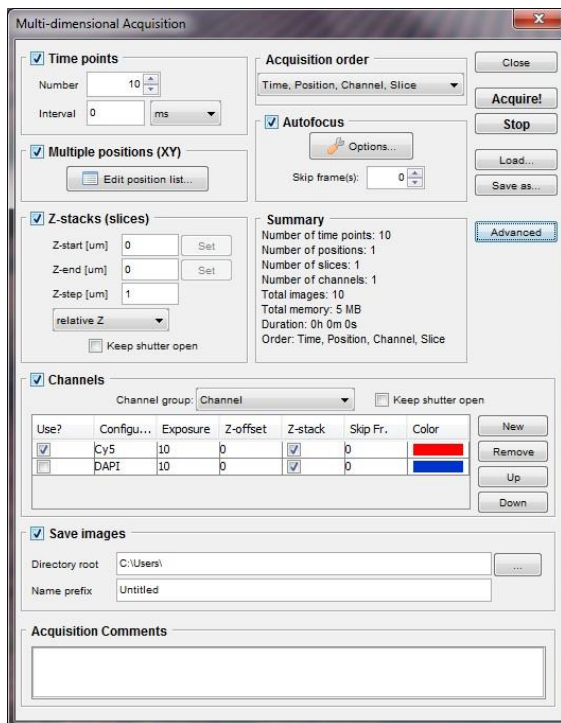


Figure 2.4. User Interface of Multi-Dimensional acquisition module of μ Manager.

2.1.4: Microscope parts and alignment:

Laser (1), with its heatsink and power decrease lenses: OBIS LS 561-50 mW Laser System, An optically Pumped Semiconductor Laser with 50 mW maximum power. This laser is controlled by the computer. Under this laser was an aluminum heatsink for it not to overheat , in front of it there are filters for further decreasing the intensity of the beam (NE13A-A - Ø25 mm AR-Coated Absorptive Neutral Density Filter and FB560-10 - Ø1" Bandpass Filter), as biological specimens are vulnerable to high intensities.

Cylindrical lens (5), ACY254-050-A with focal length of 50mm, To produce the light sheet there is the need to elongate the diameter of the beam in one dimension, a helpful addition to this lens is a rotating stage to rotate the elongation, it is need for checking if the alignment is correct or if the light sheet is thin enough.

Specimen chamber (7) with the stage (8), the acrylic chamber is custom built and able to hold the illumination lenses (2x Objective Olympus 10x, NA 0.3, WD) and detection lenses (Nikon MRP07220 Objective CFI 75 LWD 16X (0.80) water dipping). Near the chamber is the stage (Picard Miniature Smart Motors & Sensors) for 4-D rotation of the specimen (minimum step 1.5 microns, and minimum rotation 1.8 degrees). High translation speed is inaccurate, so it is not recommended for acquisition .

Detection (9), (10): ORCA-Flash 4.0 Camera a sCMOS camera with ~80% quantum efficiency in visible light and lightsheet readout mode to reduce noise of lightsheet images, maximum resolution is 2048x2048 pixels.

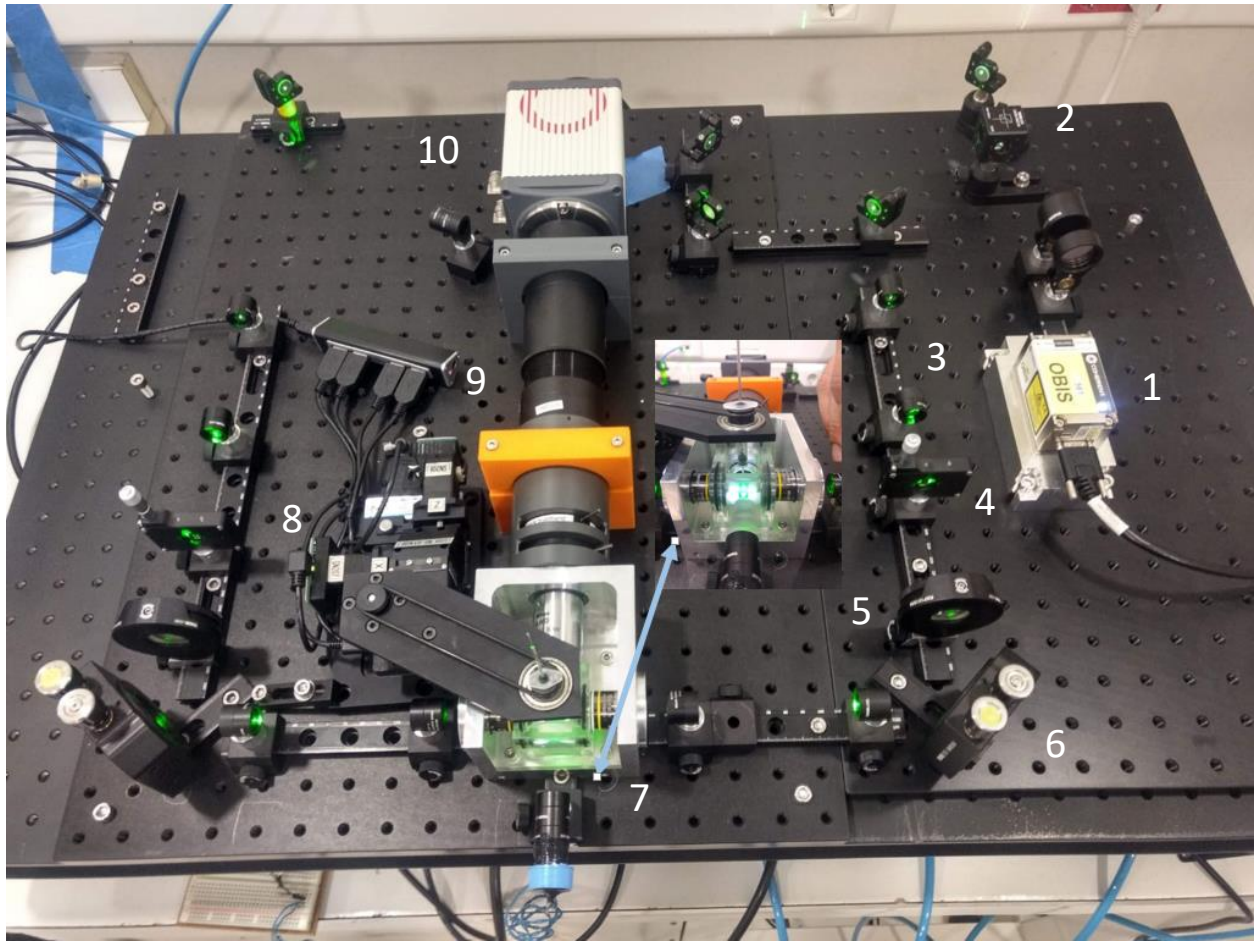


Figure 2.5. Panoramic view of the T-OpenSPIM used in this thesis. 1) Laser with an aluminum heatsink. 2) Beam splitter. 3) Beam expander. 4) Horizontal slit. 5) Cylindrical lens. 6) Precise mirror with 3 degrees of freedom (2 rotational and 1 translational). 7) Specimen chamber with 3 arms (2 illumination and 1 detection). 8) Stage with 4 degrees of freedom (1 rotational and 3 translational), 9) Focus lenses for the camera and filters. 10) sCMOS camera.

Alignment:

For the first alignment of the laser we used a frosted lens (DG05-1500-H1-MD - Ø1/2" SM05-Mounted Frosted Glass Alignment Disk), to make sure the laser beam pass through the center of each lens. Then we needed to check the light sheet width, we rotated the cylindrical lens as to produce a light sheet parallel to the floor and used fluorescent liquid to see the sheet divergence and its width, using the FWHM, the width was calculated to be ~5 μm , and aligned the 2 light sheets to overlap. Then rotating back the cylindrical lenses, using fluorescent beads, if checked both light sheets illuminated the same beads, this is important step before each imaging session, as misaligned light sheet produce data not fit for preprocessing and analysis.

2.2: Image Processing:

2.2.1: Interest Points:

After imaging the dataset is not ready for analysis all the views should be aligned so a single image can be seen, so the first step is to find the edges (Interest points) to be used for aligning the views. These interest points consist of the pool from which the possible descriptors will be chosen from to register the views.

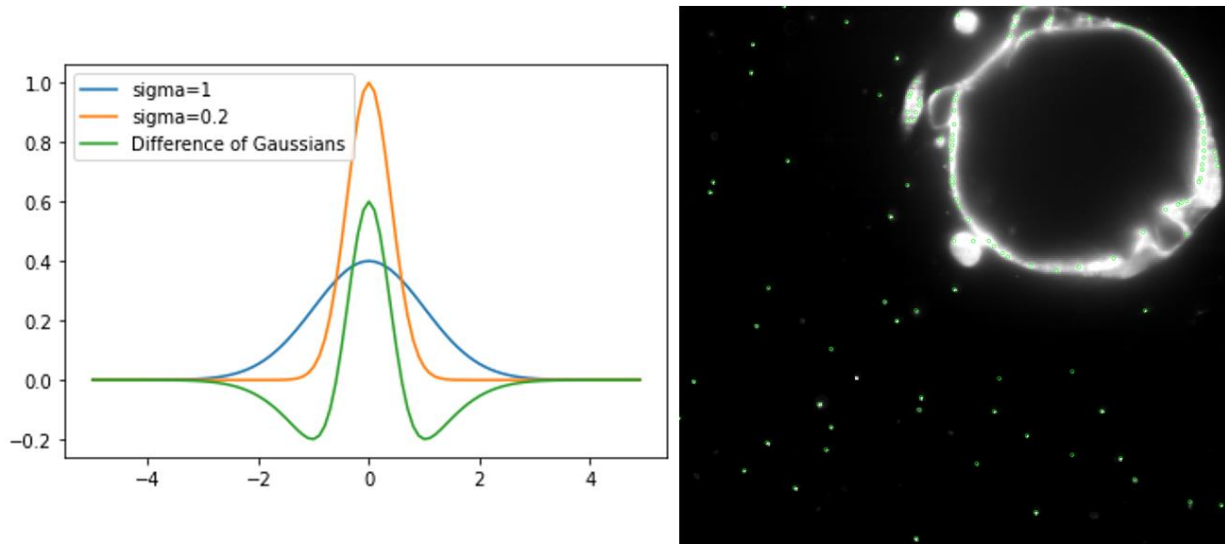


Figure 2.5. Difference of Gaussian filter and blob detection. Left image shows a graph of a Difference of Gaussian filter produced through a Python script. The DoG filter is applied on the right on a z-stack to find blobs. Both beads and parts of the specimen are detected.

2.2.2: Registration and its success:

The next step is to register the views. There are multiple algorithms available to do the registration, each with different invariance and sub-algorithms to select what transformation is to be done on the different angles. In the case there are no metadata for the program to prealign the different views, the algorithm that should be used is the rotation invariant one, because this is the only one that can rotate the views. Given the success of this step the registration process can be continued for fine tuning by selecting a translational invariant algorithm. At last there is an optional algorithm for further fine tuning, ICP (Iterative Closest Point) (Besl and McKay, 1992), this algorithm has no invariance so rotations and translations are pixel-scale. All these algorithms have multiple options to select what transformation are to be done, the options are affine, rigid and translation. Translation moves the 3-D project keeping all of its properties intact, rigid adds the rotation too, keeping angles and scale intact and affine besides all the previous can scale it and shear it keeping the lines and parallelism intact.

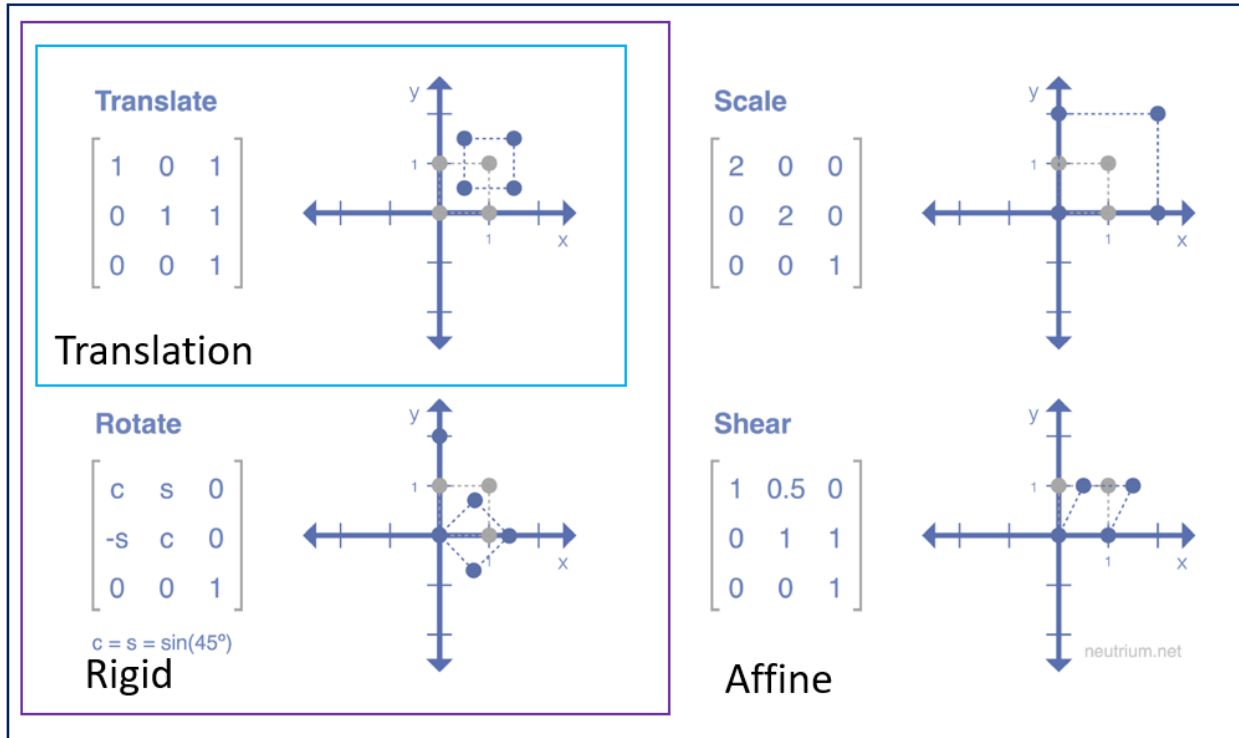


Figure 2.6. Types of linear image transformations. Each element of the matrix will be multiplied with each point on the space, so the identity matrix will do nothing on the position of the point. Translate will keep the shape and volume of the object constant and move it on the Euclidian space. Rigid transformation can do what translation can do and will rotate the object keeping shape and volume constant. c is short for \cos and s for \sin . Affine transformations can do all of the above and scale the object and keep its shape constant or produce a shear effect which keeps the volume constant but not the shape.

There is also the option to regularize the model running by using an other transformation and combining the results. All the registration algorithms are checked by a RANSAC algorithm, that will choose random Interest Points and check the error of the registration.(Foley, Fischler and Bolles, 1981).

To check the progress and to judge the success of the registrations, the log window should be checked. This window provides the average, minimum and maximum error as well as the scalings of each view in each dimension. The average error should be kept as minimum as possible and scaling near 1, as all views were taken on the same microscope with the same optical system. A more practical way to validate the success of registration, is to look if the beads are well registered, as the axial resolution of the microscope is worse than the lateral, beads are not going to be spherical, as they should be, they are oblong shaped (elongated in z-axis), giving them a new useful feature, direction. Knowing that views have a difference of $\sim 90^\circ$ or other angle, the beads too, will not fit onto each other to produce a cross or an asterisk depending on the number and orientation of the views, Figure 3.3, so if there are at least 20 that produce this shape across all the image, the registration is considered successful.

2.2.3: Fusion:

After registering the images, next is the image fusion, producing a single stack that combines all the views. However, each angle has some blurred data on the parts of the specimen where there is no uninterrupted path between the volume and the camera lens. So the fusion algorithm uses the sharpest possible data to produce the final image (content based fusion (Goshtasby, 2005)) and reduces the artifacts that are produced by registering views. This step is used only to produce deconvolved images, as I prefer to have two separate views during tracking of images, as fused images can be unreliable, sometimes.

2.3: Lineage reconstruction:

2.3.1: Mastodon:

After acquiring the images and processing them, the images are ready for nuclei tracking. The best performing program for this end is Mastodon (*GitHub - mastodon-sc/mastodon: Mastodon – a large-scale tracking and track-editing framework for large, multi-view images.*, no date) with its visualization properties and simple controls. It is the product of a long series of programs specialized for tracking, containing MaMuT (Wolff *et al.*, 2018) and TrackMate (Tinevez *et al.*, 2017). This program has the capacity to do manual, semi-automatic and automatic tracking. When in automatic mode tracking consists of 2 separate processes: segmentation and linking. Segmentation is done through the DoG filtering for blob detection, however there is no option for sigma in this case, the only values given by the user are the threshold (quality of the image, relative to the SNR) and the approximate radius of the nuclei (in pixels), so the result is spherical objects on the bright nuclei. Next, there is the option to compute set of features like spot radius, number of links, intensity... that are useful for linking and statistical analysis of the dataset. At last is the linking process, which uses a LAP Linker (Linear Assignment Problem) (Jaqaman *et al.*, 2008), which has 4 parameters, one for linking cells frame to frame, next is gap closing if a nucleus “skips” a frame or more, track division for dividing events and track fusion which is not used in this study as it will not happen in this organism, each parameter has a distance module and penalties can be added according to the features computed before.

2.3.2: TGMM (Tracking with Gaussian Mixture Models):

Another program used for automatic tracking is TGMM (Tracking with Gaussian Mixture Models). TGMM, does not differentiate linking and segmentation, they are 2 processes that are interconnected, one fixes the other and vice-versa. For segmentation a combination of watershed segmentation (Serra, 1986) and persistence based clustering (Skraba *et al.*, 2010) and linking through a “sequential Bayesian approach with gaussian mixture models” and a Nearest neighbours algorithm. So the main two parameters for using this program are threshold (conservative value to make the processing lighter and reduce the fluorescence objects that are not the focus of the tracking) and tau (value to separate two nuclei or not), both of these parameters are related to segmentation. Another feature this algorithm has is using multiple timepoints of the same specimen in parallel using earlier and later knowledge about each timepoint (early and late timepoints are not so accurate because of this) to find nuclei it may have missed. Other important parameters are : min/max NucleiSize, betaPercentageofN_k (Probability of the nucleus to remain in the gaussian curve in the next timepoint) and splitscore (probability of splitting).

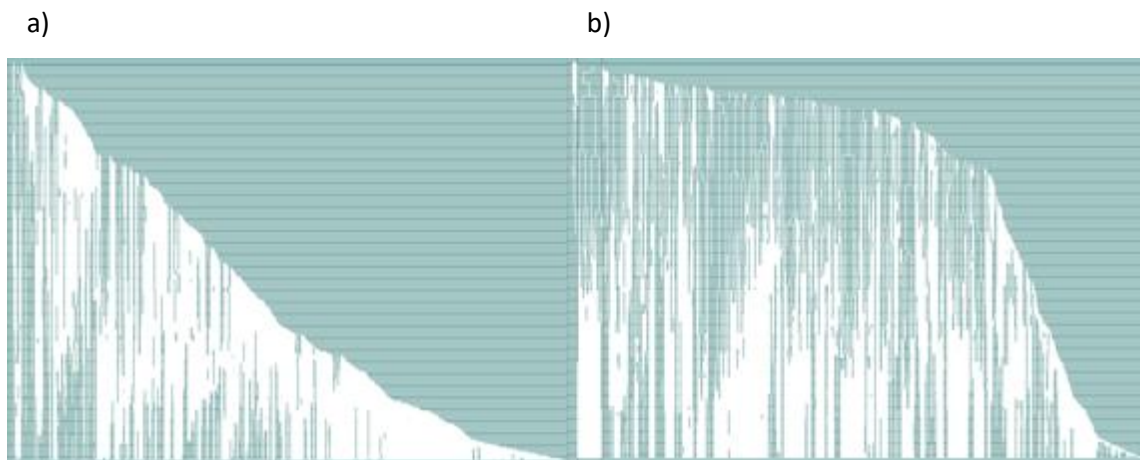


Figure 2.7. Automated and manually curated cell lineages. a) The result of automated cell segmentation and tracking with Mastodon. b) The result of automated segmentation and linking with TGMM.

2.3.3: The pipeline for producing the whole specimen:

After using both of these algorithms and having inaccurate results on *Parhyale hawaiiensis* embryos, I combining both methods and manual curation to produce the final lineages. Manual curation is easier for undersegmented with short but accurate lineages specimens than the other way around. So, using TGMM and finding the best parameters for under-segmentation and linking, through trial and error, I produced a dataset with ~40% of the nuclei segmented and multiple correct 30 timepoint lineages. Afterwards, the results are imported to Mastodon and I try one more under-segmentation adding even more nuclei and then through the linking algorithms and linked them with 30% track accuracy. The final result came through thorough manual curation. The main controls are: add a new spot, remove one, add next/previous spot (linked to the previous/next), spot linking. The best pipeline for manual curation is first to check if the existing tracks are precise, if not fix the links or delete them completely, as its not worth to correct a track with 50% accuracy or less. I preffer having 2 perpendicular views of the sample to make sure that I have tracked the right nucleus, one that focuses on the surface and one that show the interior of the egg, as well the cell focused. For later curation the trackscheme is important too, as it can be used for a qualitative check on the divisions, because the focused lineages have a similar division pattern, so a missing division is a great indicator.

3. Results

3.1: LSFM (Light-sheet Fluorescence Microscopy):

3.1.1 LSFM images

The main specimens used for imaging were of *Parhyale hawaiiensis* embryos and digestive system, using a T-SPIM microscope (2 illumination arms and 1 detection arm). Some specimens were larger than the FOV (field of view), so images were taken with an overlap of ~30% to stitch them afterwards. All specimens were imaged along with beads, due to their serving as a position system and point sources to be used for deconvolution. The gut system was dissected, fixed and stained with a conjugation of Rhodamin-Phalloidin or Congo red. Phalloidin is a peptide that binds on actin filaments, Rhodamin is used as a fluorescent dye coupled to Phalloidin producing an aggregate that binds on actin (*Phalloidin staining protocol* / *Abcam*, no date), Congo red stains chitin (Yakupova *et al.*, 2019).

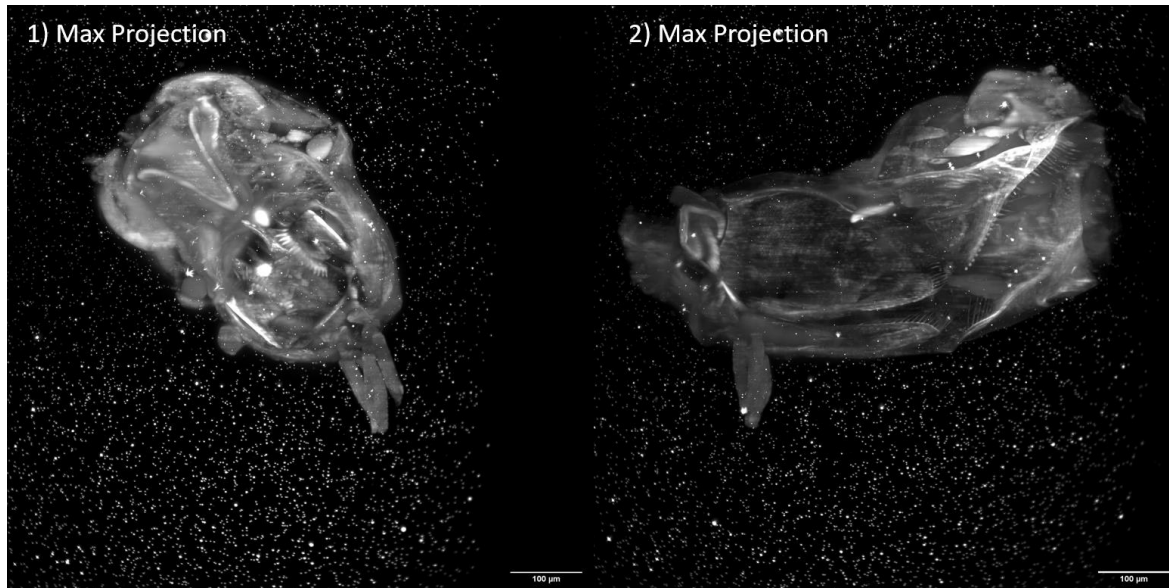


Figure 3.1. Multi-view LSFM acquisition of the *Parhyale* foregut. a) Ventral view of the foregut (tubular esophagus and bipartite stomach) and b) lateral view of the same specimen rotated by 90°. Images show maximum intensity projection of the dissected foregut stained with Congo red, imaged with voxel resolution 0.4x0.4x3.0 μm^3 and embedded in low melting agarose with 500 nm bright fluorescent beads (FY Estapor, 1398/42/45).

To showcase the difference in spatial resolution between views, two perpendicular angles are focused on the same part of the stomach. The small spherical particles (~450 nm) around the specimen are called beads, these beads are visible in Figure 3.1, Figure 3.2 and Figure 3.3 in most detail.

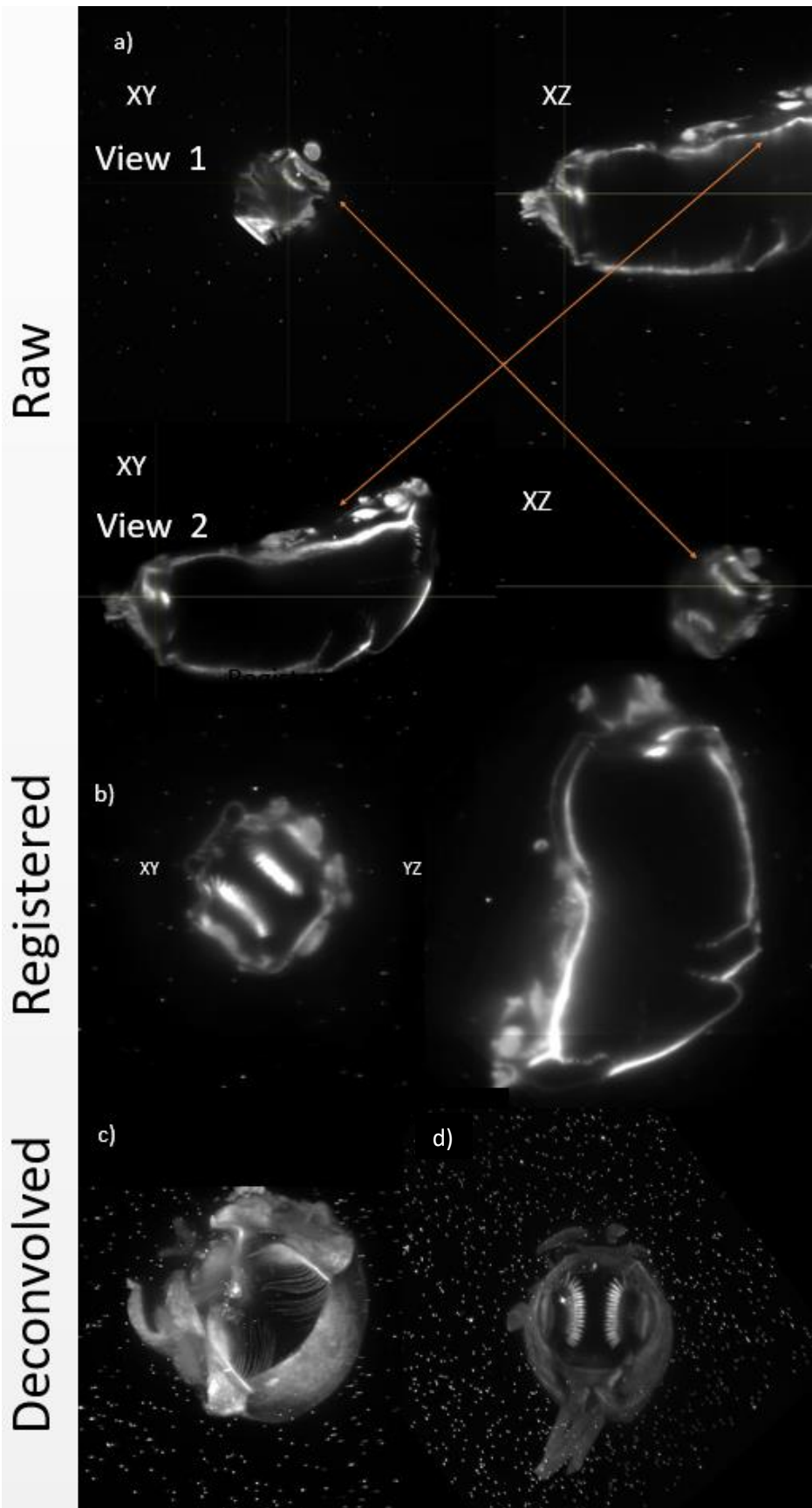


Figure 3.2. Raw, fused and multi-view deconvolved LSFM images. The same two optical sections of the *Parhyale* foregut, a cross-section through the filters of the esophagus (left) and cross-section through the stomach (right) are shown in a) xy and xz slices from the first raw view, arrows indicate that two different views have different resolution across the specimen b) xz and xy slices from the second raw view that is perpendicular to the first view, c) the registered and fused images by simple content-based fusion, and d) the registered and fused images by more advanced multi-view deconvolution.

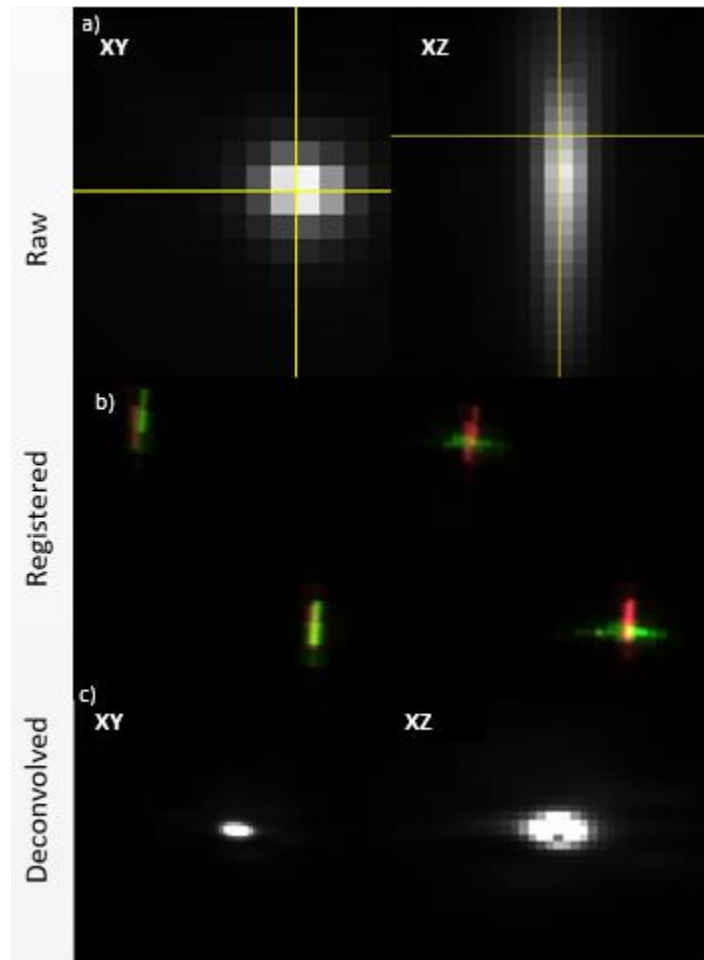


Figure 3.3. Orthogonal views of fluorescent beads in raw, fused and multi-view deconvolved LSFM images. a) Lateral xy (left) and axial xz (right) optical sections through a fluorescent bead in raw LSFM images. The bead appears as a point source with a radius of few pixels laterally and an oblong shape several pixels long axially. b) xz view of correctly registered beads. Left view the two images of beads will overlap. On the right image using 4 views the overlap will produce a small cross. c) Lateral xy (left) and axial xz (right) optical sections through a fluorescent bead in fused LSFM images by multi-view deconvolution with an almost isotropic resolution.

For the last example of images, I would like to focus on large specimens. These large specimens are far larger than the FOV, so the aim is to image smaller, overlapping parts and then stitching the multiple tiles. Thus, by making the acquisition more time consuming, we can produce an image of the whole large specimen without changing magnification and sacrificing resolution, Figure 3.5.

Another microscope was used to produce images of embryos developing, SimView (Tomer *et al.*, 2012) which has many functionalities that improve image acquisition, like another camera opposite of the first one (X-SPIM like) and autofocus galvano-mirrors, which allow long acquisitions without external disturbances, like aligning the light sheets by hand in-between timepoints. These, datasets were acquired by Valia Stamataki and Leo Blondel in *Janelia campus* (HHMI).

3.2: Image Processing

3.2.1: Introduction:

Raw LSFM images have good lateral resolution and great optical sectioning, however the subpar axial resolution and the blurry parts on volumes that cannot be seen directly by the camera can be enhanced using other views. There are two pipelines used for the production of fully processed images: One is a general pipeline, that uses beads as small points of reference and can fuse multiview images produced by any microscope. The second one that is designed for SimView-like systems (2 cameras), and does not need any additional information, like beads. This part will show the results of each algorithm and a comparison between them.

3.2.2: Multiview-Reconstruction:

The first step to use this program is to import all the image files, which have the format `Tile{number}Angle{NUMBER}`. Then it is recommended to resave the files as HDF5 format (Koranne, 2011) to reduce the data volume and enhance reading speed. Then, interest points are found in each image by convolving the image with a Difference of Gaussian filter using specific threshold intensity and sigma value, these interest points can either be beads or parts of the specimen. Beads are far more reliable, so through the program I reduce the detections on the specimen, according to distance between detections.

3.2.3: The results:

Through trial and error an appropriate registration pipeline was produced. First a rotation invariant affine with a rigid regularization (λ 0.05), then a translation invariant rigid with an affine regularization (λ 0.05) and for the last step, an ICP affine registration as the views will be mostly aligned. Modifications of this pipeline can be made for more difficult samples. The sample you can see in figure 3.2 is a stomach imaged from 8 different views and registered through this algorithm. A subtle imperfection is apparent in the figure 3.2 b, as the intensity falls off abruptly, this happened, because each view does not contain the whole specimen, but a segment of it.

3.2.4: Time Drift:

All these processes are for spatial registration, however for time-lapse imaging, like developing samples, it's a requirement for the specimen to remain stationary in its place, because analysis of a time-drifting embryo, especially in tracking can prove a difficult or even impossible task, this effect is shown in Figure 3.4. This could be fixed by making the microscope as stable as possible, however during long time imaging (1-3 days) even the most stable microscopes tend to misalign themselves through its own movements. Thankfully, beads once again are used to provide stationary points of reference to register the whole image.

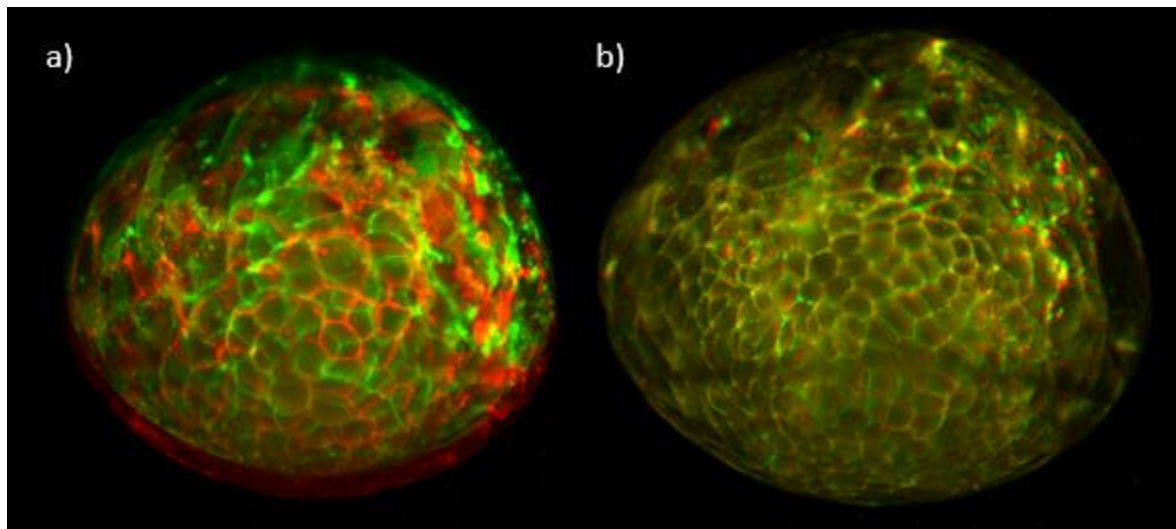


Figure 3.4. Temporal registration for time drift correction. a) Maximum intensity projections from consecutive time-points 156 (green) and 157 (red) are shown superimposed, these two timepoints were not registered correctly b) Maximum intensity projections from consecutive time-points 182 (green) and 183 (red) are shown superimposed, these two timepoints are registered.

To fix time drift the same registration processes are applied, but across timepoints.

3.2.5: Stitching:

Some specimens are larger than the FOV, so the need to acquire parts of the specimen and then stitch those images has risen, that way the images keep both the advantages of a smaller FOV with great resolution and the whole specimen can be seen, losing only time efficiency and data volume. Each tile is a translation in one of the spatial axes (sometimes a small rotation too) so the most optimal way to solve this problem is to use specific algorithms that deal with such transformations to reduce the computational time. For stitching I used the program BigStitcher (Hörl *et al.*, 2018), which uses a phase correlation method (Kuglin, C. D. and Hines, D. C., 1975. The Phase Correlation Image Alignment Method. Proceeding of IEEE International Conference on Cybernetics and Society, pp. 163-165, New York, NY, USA.). This method uses the Fourier

transforms of the images and Fourier shift theorem combined with a phase correlation function. The correlation function will produce a 3-D plot with many peaks and the program tries to identify which peaks provide the greatest correlation. This method was modified to fit rigid and affine transformations, so a tile that with subtle rotational misalignment ($\sim 1^\circ$) is possible to register successfully. Again ICP can provide fine adjustments for subpixel accuracy. Then the tiles are registered with the previous algorithm. An example of stitching is this sample of a *Parhyale hawaiiensis* gut Figure 2.8, which was imaged for 5 different tiles (4 angles each tile, so 20 views summed up).

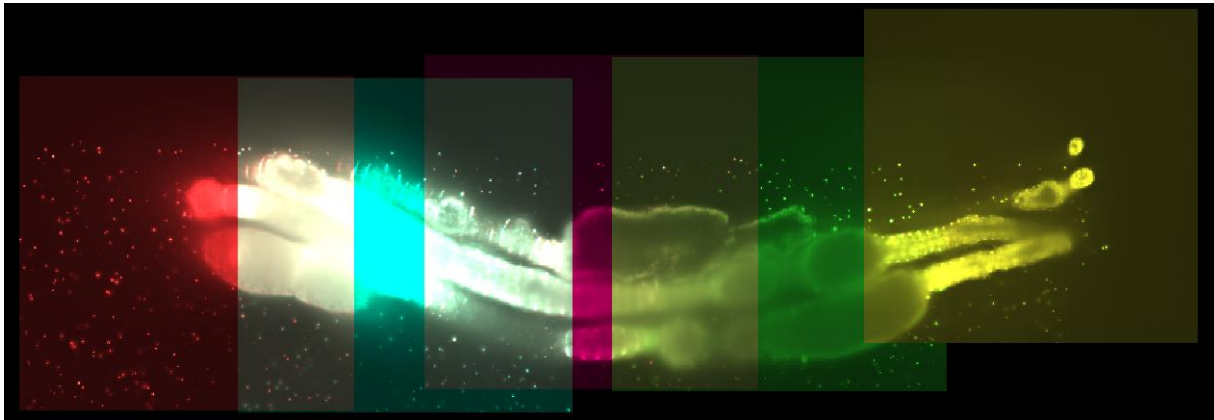


Figure 3.5. Tiled rendering of the entire *Parhyale* digestive system. Each colored rectangle is a different tile with minimum 15% overlap with neighboring tiles. The dissected and fixed *Parhyale* digestive tract was stained with rhodamine phalloidin (staining filamentous actin) and was embedded in low melting agarose with fluorescent beads (FY Estapor).

3.2.6: Deconvolution and Results:

Any image acquired from an optical system is not perfect, even human eyes, it's a blurred image produced by the interaction of the whole optical system with light sources, this effect is called the Point Spread Function (PSF). Many algorithms have been produced to uncover the real image behind the blurred one (Verveer and Jovin, 1998; Agard, 2003), however the algorithm that was used should be applicable to 3-D images so the chosen one was Lucy-Richardson iterative deconvolution algorithm (Richardson, 1972; Lucy, 1974). The convolution equation is:

$$\varphi(x) = \int \psi(\xi)P(x|\xi)d\xi$$

where $\varphi(x)$ is the result image and $\psi(\xi)$ the “real” image convolved with the PSF ($P(x|\xi)d\xi$), so defining the inverse probability $Q(\xi|x)$, we can solve the equation for $\psi(\xi)$. However there is always random noise which is unknown, to overcome this problem the method uses iterations producing better results with each one. This is a deconvolved image stack from a stomach of 8 different views, as it is apparent, many subtle, hidden information is ‘uncovered’, Figure 3.2. And the projections of the beads have changed to more spherical particles Figure 2.3.

2.2.7: Keller pipeline:

The other series of algorithms used for image processing are the Keller algorithms (Amat *et al.*, 2015), which are algorithms for light sheet microscopes with 2 opposite detection arms and 2 illumination arms. These algorithms use the klb format (Keller lab block), a lossless format inspired by the linux Parallel BZip2 (Gilchrist, no date) compression technique, it provides better performance speed and less volume on the disk. The first step of this pipeline, is called ClusterPT and finds dead and saturated pixels and replaces them with the mean of their neighbours and a background image can be subtracted, if needed, the image can be cropped and then resaved as a klb file. Next is ClusterMF, which connects the 2 views using masks every n timepoints (n should be an interger ranging from 5-15 according to the quality of the dataset), then localAP extracts the parameters and ClusterTF applies them to all the timepoints, to check if the specimen is well fused The yz or xz projection should be checked if it giggles (the 2 views get further from each other and the near again producing a accorden effect), in case of failure this step should be repeated for less timepoints. Last is ClusterCS that fixes time drift and normalizes intensity, however very abrupt and big movements, may make the specimen too difficult for the algorithm to fix as it uses a center of mass mask to stabilize the embryo. This set of algorithms is much faster than Multiview Reconstruction, however it cannot fuse views that are perpendicular to each other and time drift correction is not always on par. So using both algorithms a new pipeline was made to have the best results the fastest way possible. The results are the same, for opposite views, however, if more views are to be involved this script will not work.

3.3: Lineage Reconstruction:

3.3.1: Introduction to lineage reconstruction:

Embryos are an ever changing series of interactions between DNA, proteins and whole cells with eachother, producing huge networks and feedback loops. Due to the difficulty and vastness of these networks an embryo cannot be studied on just molecular level, there is a demand to study its development and cell fate through morphological means, producing lineages, which show the positions, movements and divisions of the cells. The first work on lineage reconstruction was done on *C. Elegans*, as it has a limited amount of cells and very specific division times (Sulston *et al.*, 1983). These morphological studies are useful on mutated or ablated embryos too, as the coping mechanisms of the embryo can show in great detail the behaviour of the embryo and when this would occur. Thankfully, nowadays we have access to modern tools like, 3-D images and tracking software to make annotations directly on the data.

3.3.2: Datasets:

For this dataset a wild type embryo was imaged during its first 3 days of development (16-1200, cells, consisted of 367 timepoints, one every 10 minutes), the imaging ends after the embryo has reached the grid stage, its volume is 196 GB after cropping and resaving as klb format. It contains 2 opposite views taken from SimView, however they were not fused into one image, because the registration was subpar. For tracking I used two views simultaneously to have vision of the 3-D volume around the cell to be tracked. Artifacts, Figure 3.7, exist in later stages of development data.

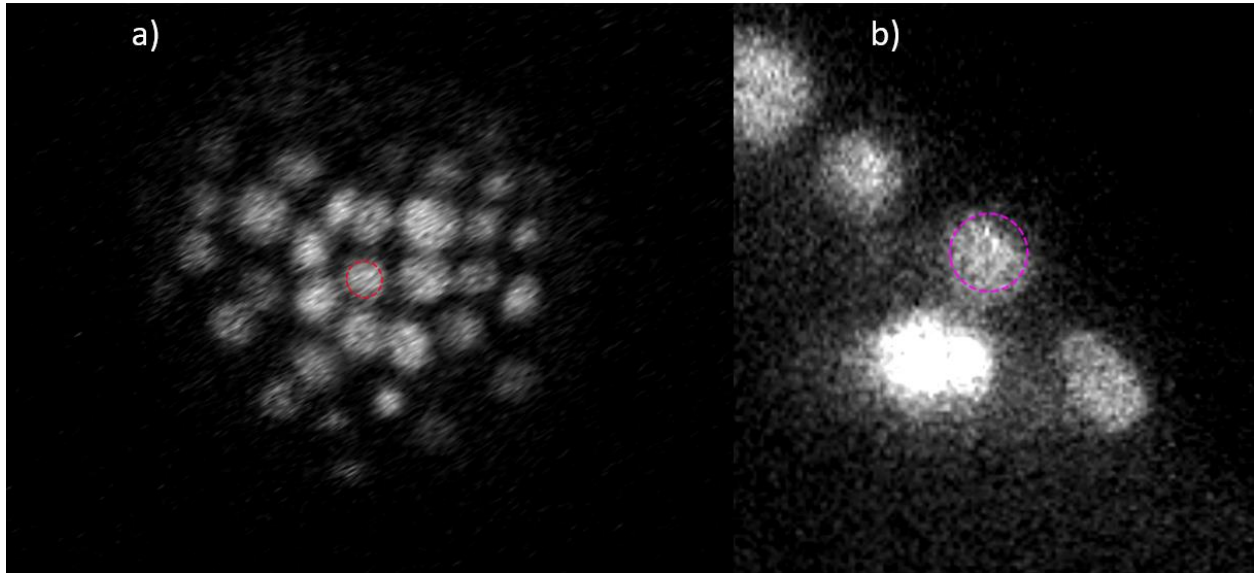


Figure 3.6. Nuclear tracking for cell lineage reconstruction. Accuracy of tracking is ensured from visualizing each segmented nucleus (indicated with magenta circle) from linked orthogonal sections. a) Lateral xy view and b) perpendicular yz view.

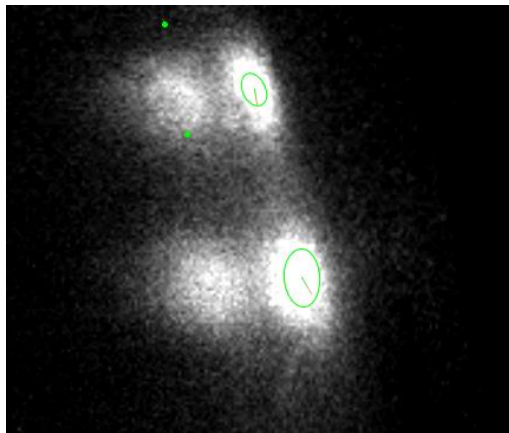


Figure 3.7. Artifacts produced by the light sheets in XY view. The nuclei to be tracked are on the surface (green circle) and the artifacts seem like another nucleus just behind the other.

These artifacts (Figure 3.7) should be a product of misaligned light sheets and they were visible in both specimens. Sometimes cells would form similar aggregates, however after some time they will separate.

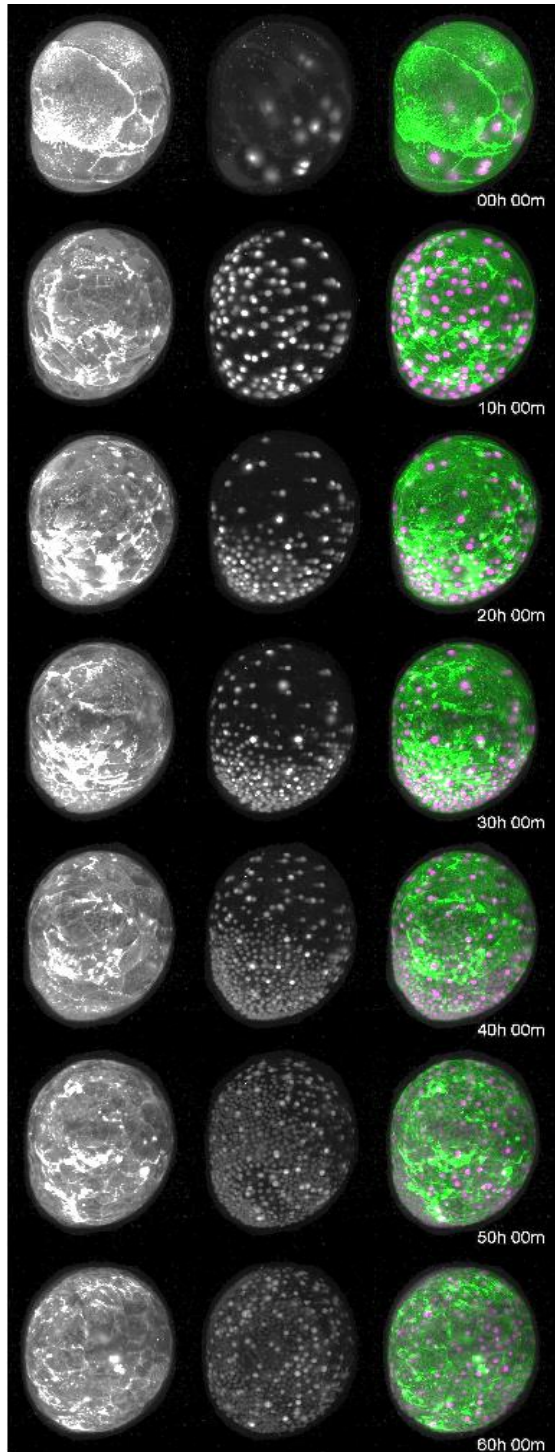


Figure 3.8. Time-lapse LSFM imaging of early *Parhyale* embryogenesis. Maximum intensity projections of a doubly labeled embryo with fluorescent membranes (left column), fluorescent nuclei (middle column) are shown individually and merged (right column) from early cleavage stage (top; 10 hours after egg lay) until mid germband stage (bottom; about 70 hours after egg lay).

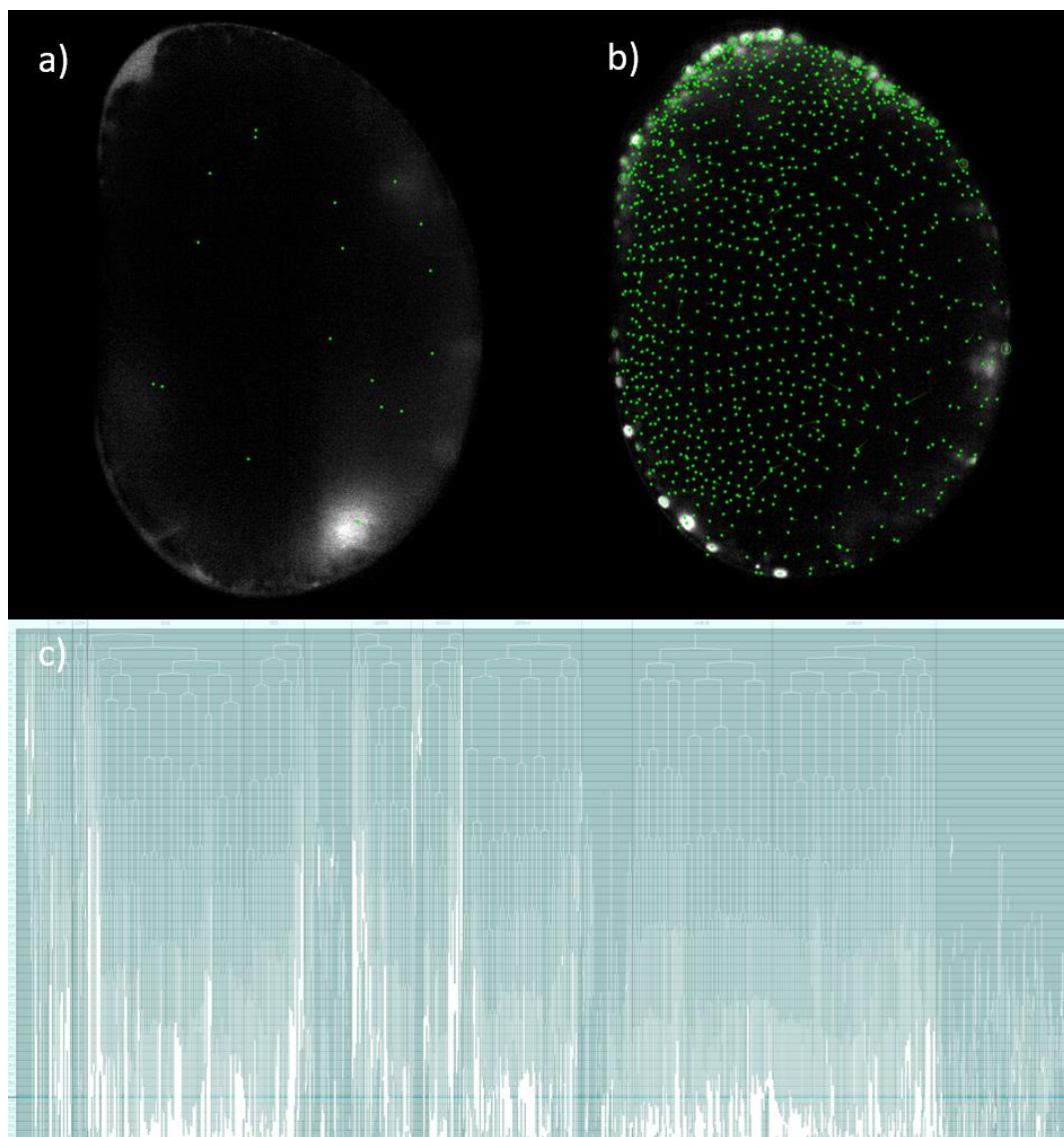


Figure 3.9. Lineage reconstruction of a wild type embryo. a) The first timepoint and b) the 319th timepoint of the imaged embryo. Green dots correspond to the tracked nuclei. c) Lineage tree showing all tracked nuclei of the embryo. The different tracked nuclei are arranged along the x-axis and their divisions are indicated during developmental progression along the y-axis (top-to-bottom).

3.3.3: The development of the embryo (a short introduction):

Like all embryos, *Parhyale hawaiensis* eggs start with just one cell, filled with the protoplasmic region (nucleus and cytoplasm) and yolk, 4 hours after fertilization a total cleavage takes place separating the cell to two slightly unequal parts, 2 hours later both of the cells divide slightly unequally producing 4 cells. Afterwards another largely unequal cleavage will produce 8 cells, 4 macromeres and 4 micromeres, each division is perpendicular to the previous one. Each of the blastomeres in this 4th stage of embryogenesis, is committed to a particular cell fate (Ep (Ectoderm posterior), El/r (Ectoderm left/right), Mav (Somatic mesoderm anterior and mesoderm visceral), ml/r (somatic mesoderm), en (endoderm), g (germ line)). The main focus of this study is the ectoderm, as it remains on the surface of the embryo during the span of my dataset. During the next stage asymmetrical cleavages cause the yolk to aggregate into the interior of the embryo and the ectoderm cells have a faster rate of division than all other cells, then all the cells remain on the surface and have approximately the same size and same distance between each other, this stage is called soccerball stage. After this the cells will migrate to the ventral-anterior part of the embryo, forming the rosette, this event is called gastrulation, the formation of the germ disc. After they proliferate they start coming back down to form the midline and the grid, a highly organized structure, that contains rows and columns of cells with a middle column demarcating the ventral midline (Gerberding, Browne and Patel, 2002; Browne *et al.*, 2005).

After 6 months of tracking, finally a Wild Type embryo was fully tracked. Two programs were used for this work, Mastodon and TGMM (Tracking with Gaussian Mixture Models (McDole *et al.*, 2018)). So this section here is important to discuss the results of this work.

3.3.4: Population graphs and analysis:

Using the features produced by mastodon and the python libraries numpy, pandas and matplotlib, I produced graphs to connect populations change and division rate changes with critical events happening during embryogenesis, the events are, stage 5 (timepoint 0-25), “soccerball” stage (time 25-50), the anterior migration (timepoint 50-99), the anterior proliferation/rosette stage (timepoint 99-166), posterior migration (timepoint 166-330) and grid formation (timepoint 330-350). These stages are shown in each figure in this section.

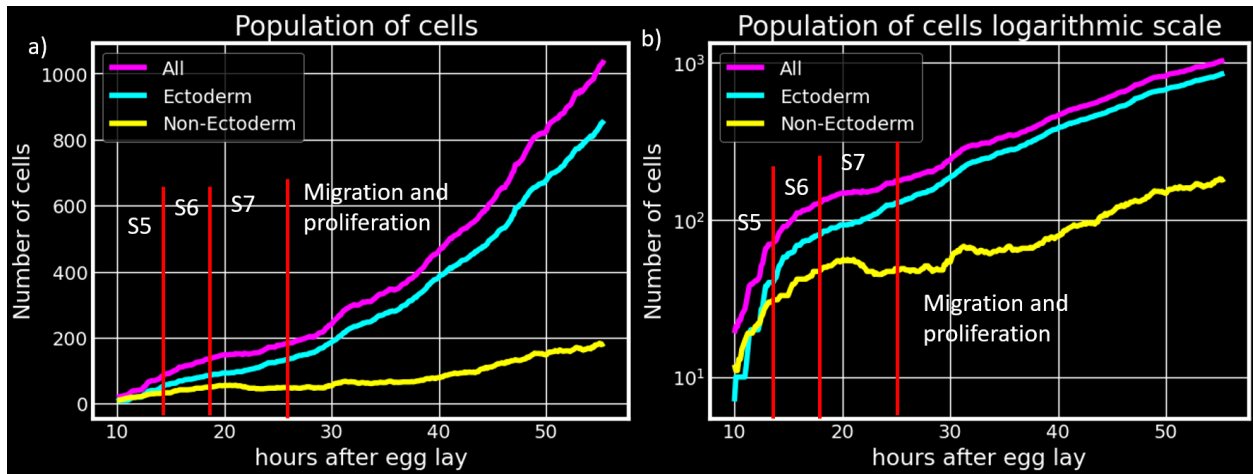


Figure 3.10. Number of tracked cells in wild type embryo. Graph showing the number of all cells, ectodermal cells and non-ectodermal cells tracked over time (in hours after egg lay). Red bars indicate the timing of developmental stages S5, S6 and S7.

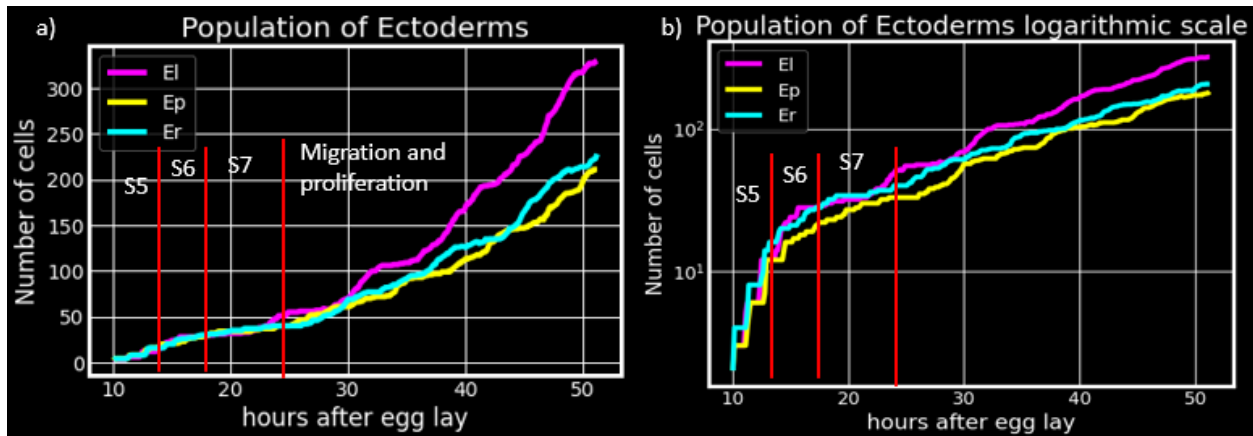


Figure 3.11. Population of each ectoderm lineage. Graph showing the number of tracked cells over time (in hours after egg lay) in each ectodermal sub-lineage. Red bars indicate the timing of developmental stages S5, S6 and S7.

The Er lineage appears smaller than its symmetric lineage El. It is apparent in the grid view, figure 3.13 that Ep has taken a substantial part of the Er family in the grid. This inconsistency may be fixed during the later stages of development, however I have no data to test if this will happen.

Focusing on the whole population of cells we can see even more interesting results, figure 3.10. The main part of all the population is of ectoderm lineage for these timepoints, the rest is descendants of the other five lineages. Their proliferation and movements can only be tracked at the start of embryogenesis as these cells will migrate towards the interior of the egg remaining unseen for a great part of embryogenesis.

3.3.5: Migrations:

One important thing is to see the migrations of the cells and in particular the migrations before and after the rosette stage. After the “soccerball” stage, cells begin to migrate towards the anterior Figure 3.12 a), there the division rate comes to a near halt, and this may be an indicator of gastrulation actions taking place. Afterwards the cells start proliferating again, remaining, however, on the anterior/head part of the egg. Sometime later the cells will start their migration to the posterior, forming an interesting structure, called grid.

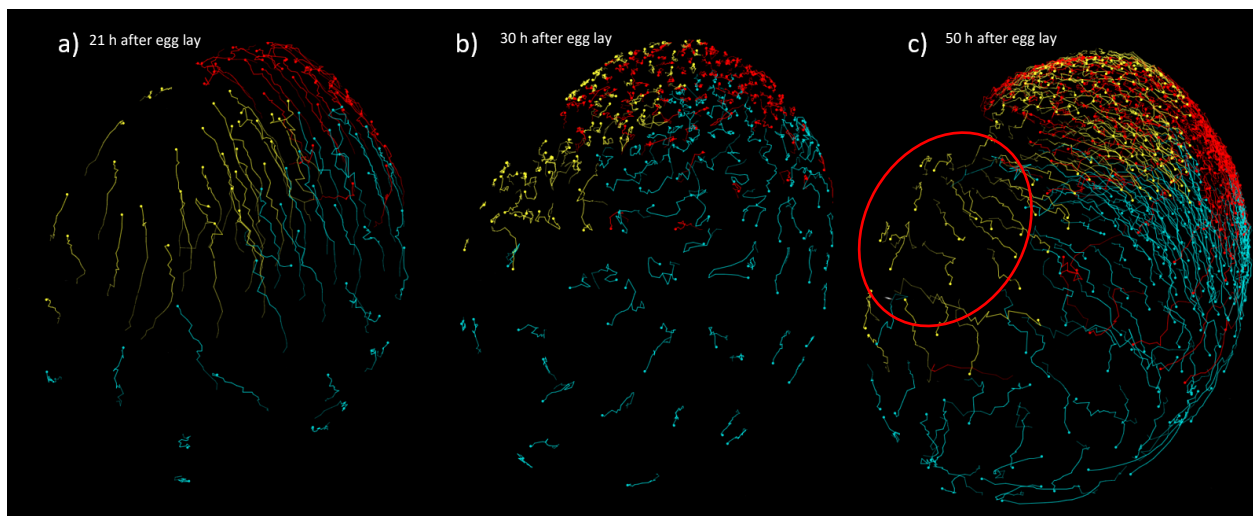


Figure 3.12. Migration patterns of ectodermal cells. a) During germ disc formation, ectodermal cells migrate to the anterior-ventral part of the egg (8-21 hours AEL). b) Migration ceases and cells start proliferating exponentially (21-30 hours AEL). c) The vast majority of cells migrate posteriorly during germ-band formation and elongation (30-50 hours AEL). Each color represents one of the three ectodermal sub-lineages: Ep in cyan, Er in yellow, El in red. Only few cells of ectodermal origin (some indicated with the red circle) remain on the dorsal side and give rise to the extraembryonic membrane. All images show lateral views with anterior to the top and ventral to the bottom.

3.3.6: The Grid:

This grid structure, which is the last part of my dataset, has some very specific features:

- A column of cells lays in the middle of the structure, called midline. This midline consists of a cell originating only from Ep family and the bulk of it will be produced by a cell produced in the 4th division of Ep (after this cell receives its fate), shown on Figure 3.13.

- The ventral midline segregates the two ectodermal lineages Er and El. Data shows that the two lineages are not symmetrical.
- Orange line is where the cable exists, a structure that segments the head region and the trunk region
- When midline ends, the head region begins, in this region there is intermixing between the two families.
- Left and right of the grid there are columns of cells of each corresponding family. On the most anterior part, the columns are 5, reaching greater numbers in the posterior part of the grid.

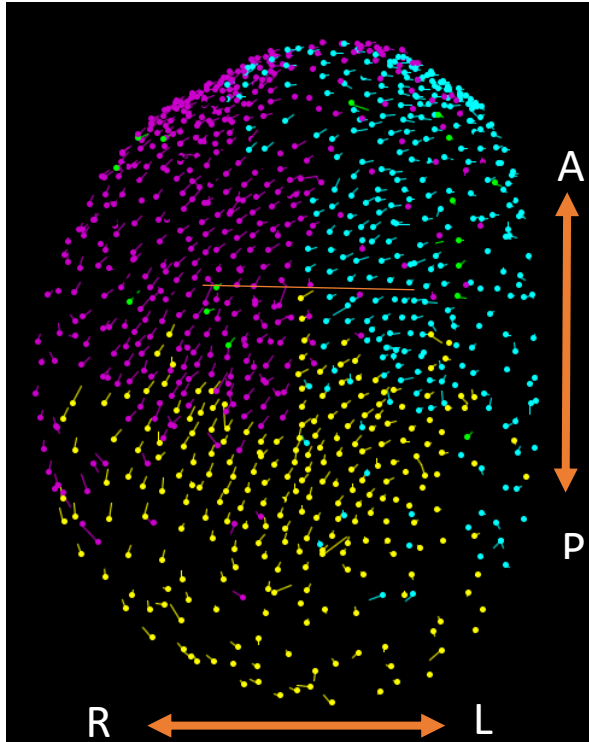


Figure 3.13. Clonal contributions in the *Parhyale* ectoderm. Mastodon toy model of the color-coded contributions of each of the three ectodermal sub-lineages: El in cyan, Er in magenta, Ep in yellow. Each spot corresponds to a tracked cell from early cleavage until mid-germband stage shown here. Ventral view.

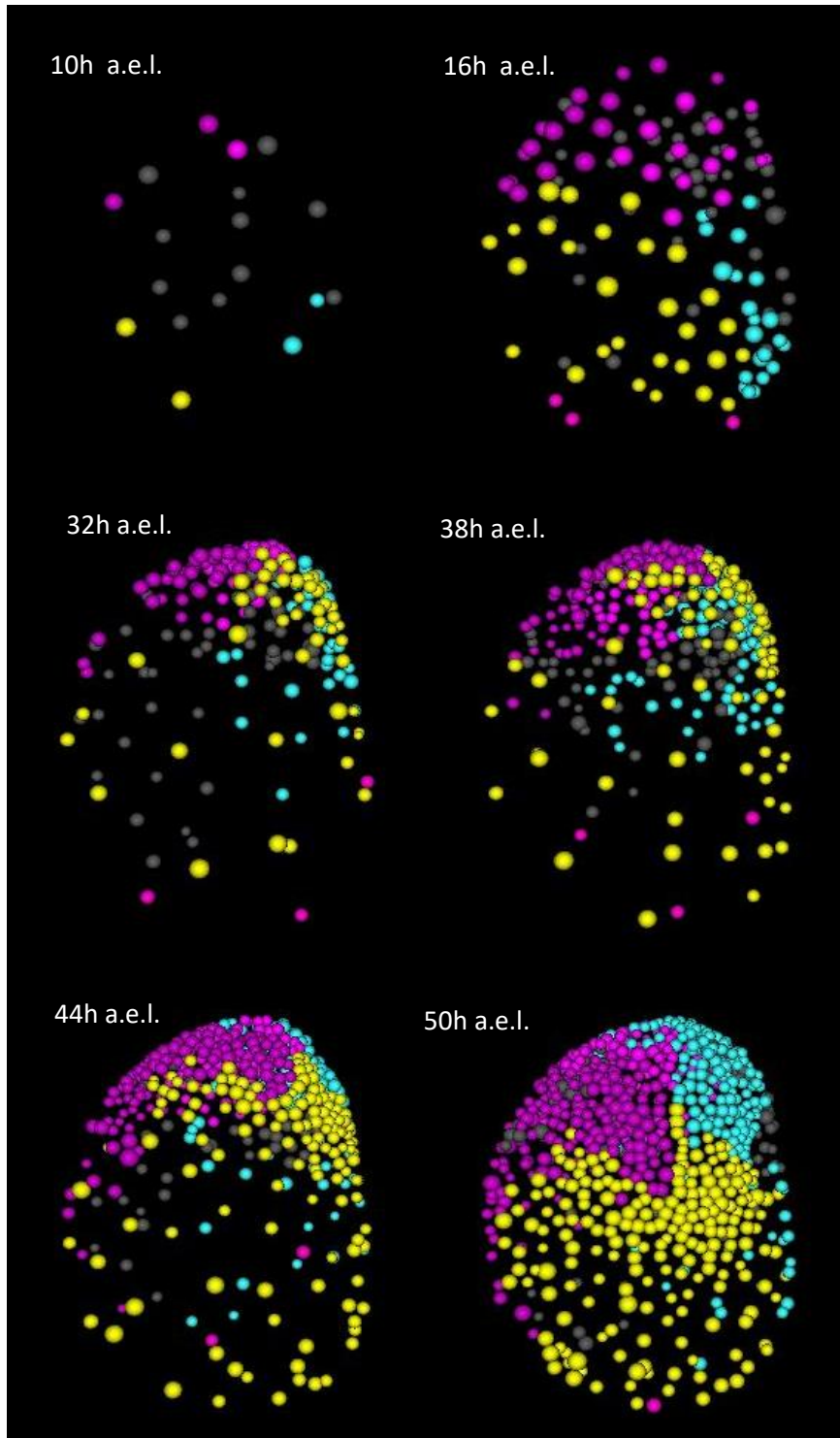


Figure 3.14. Time-lapse toy model of all tracked cells in the wild-type *Parhyale* embryo. Non-ectodermal cells are shown in gray and ectodermal cells are shown color-coded according to their origin: Ep derived cells in cyan, Er cells in yellow, El cells in magenta. All images show ventral views with anterior to the top and posterior to the bottom.

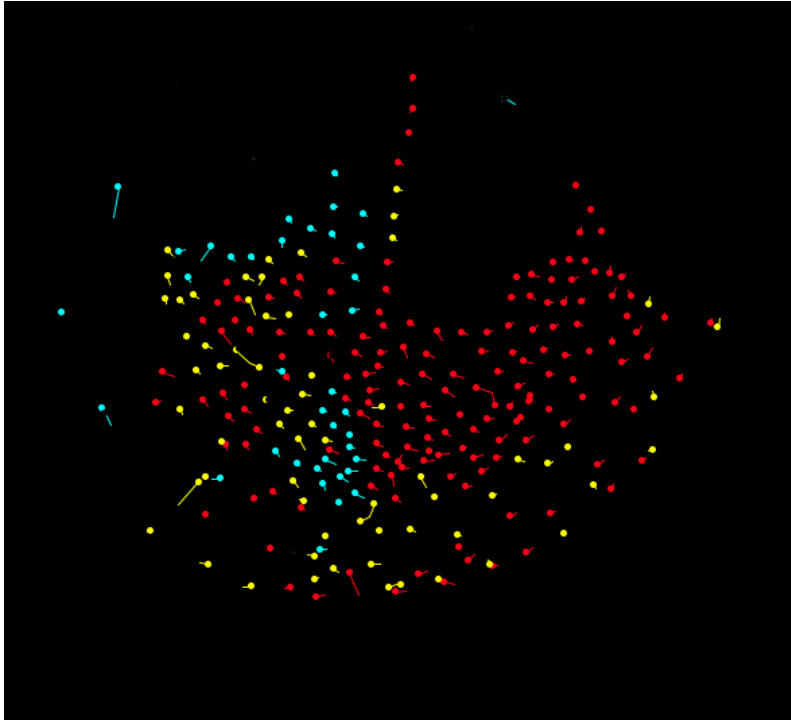


Figure 3.15. Clonal contribution of Ep descendants to the *Parhyale* ectodermal grid. Toy model of tracked Ep cells in the mid-germband stage showing the contributions of the two Ep daughter cells, Epr (shown in cyan) and Epl (shown in red and yellow). The Epl daughter cells contribute to the ventral midline and most of the posterior grid. Ventral view with anterior to the top and posterior to the bottom.

3.3.7: Neighborhood divisions:

During the development of the embryo, a strange pattern is apparent during multiple timepoints, a small number of neighbouring cells will divide simultaneously, having the same spindle axis, Figure 4.16, not to be confused with the division of rows in grid stage. The same axis divisions may happen between the 15 and 40 hours of development on the ventral side of development. This event happens only on one cell lineage each time.

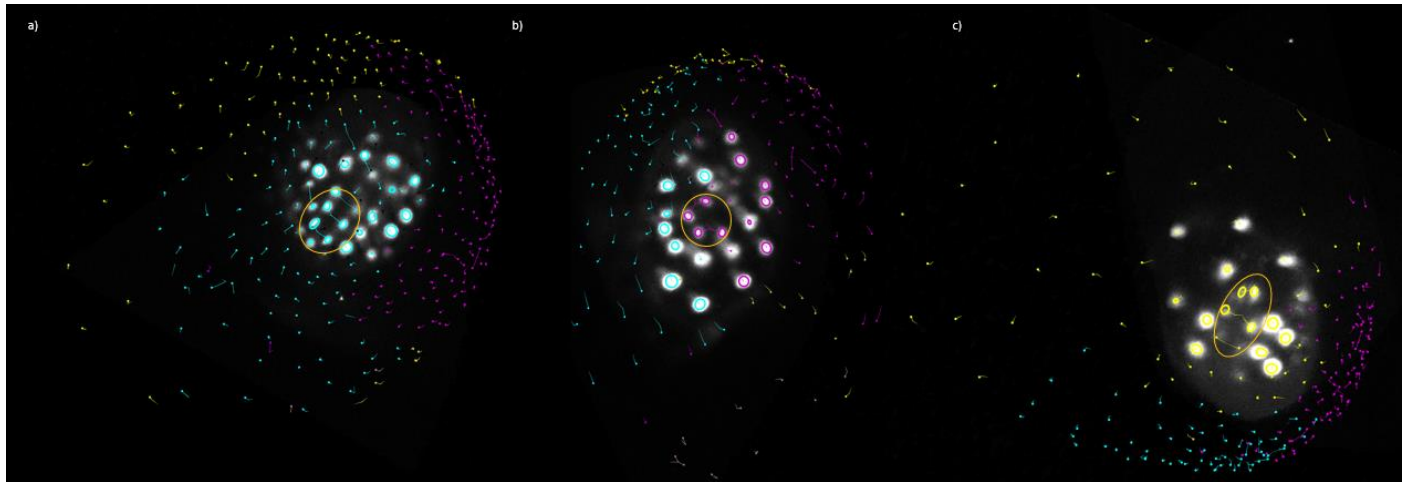


Figure 3.16. Putative mitotic domains in the *Parhyale* ectoderm. Orange circles indicate groups of neighboring cells dividing simultaneously. a) E1 cells ~50 hours after egg lay. b) E2 cells ~38 hours after egg lay. c) E3 cells ~34 hours after egg lay.

4. Discussion:

The diversity of crustacea is a great area for evolution, developmental and regeneration studies. Both gene level and morphologic research is important to build the whole network of interactions from one cell to full grown animal.

This tracked embryo provided more detail on the early development of *Parhyale*, so it's appropriate to compare it with similar studies of early cell fate specification. Browne (Browne et al 2005) indicates that ectoderm cells have higher proliferation rates than other lineages, as it can be shown in Figure 2.19. The early anterior axis is shown by the first migration of the cells, however in experiments not shown here the anterior-posterior axis is specified by the S4, left-right or dorsal-ventral axes are not indicated that early. The rosette cells move under the ectoderm, due to the low depth of the imaging I am not able to determine their fate afterwards.

As similar work has been done to other organisms, like *Orchestia cavimana* (Scholtz and Wolff, 2002), there should be a comparison between these organisms. The first cleavage of both organism is total and produces 2 slightly unequal cells. The next cleavages of both organisms are all meridional. The 8 cell stage consists of 4 macromeres and 4 micromeres and each cell has a specific fate. The fate of each cell and their shape in *O. cavimana* are very similar to *P. hawaiiensis*. The first great difference between the 2 organisms is the gastrulation stage, where a blastopore is visible on the *O. cavimana* egg. Still similar to *Parhyale* both organisms will form a grid like structure (Wolff and Scholtz, 2006).

Another important step to continue this project is producing higher quality images with greater depth, less artifacts and greater temporal resolution. New LSM technologies can provide solutions to these problems. Conventional light sheets may produce images with artifacts like the ones in Figure--, so producing light sheets with scanning mirrors is the best solution to have a clear image, this will produce a "multi-angle" light sheet that will eliminate such artifacts. New cameras needing less exposure to the specimen making the acquisition faster, simultaneously using 2 cameras like X-openspin and Simview (Tomer *et al.*, 2012; Girstmair *et al.*, 2022) or even 4 like the isoview microscope (Chhetri *et al.*, 2015) will lessen or even eliminate the need for rotation, which means less time wasted for repositioning the embryo. Another enhancement important for developmental research is depth imaging without using more intense light sources, because biological samples are very vulnerable to intense light. Recent advances in physics may be a solution to such a problem, one such advancement are photon bullets. The most important feature of these bullets is that they can illuminate a specific segment of a volume they are targeted to, without interacting with the rest of the volume. (Abdollahpour *et al.*, 2010; Chong *et al.*, 2010; Vettenburg *et al.*, 2014). The last problem light sheet microscopes may have, is the fact that light sheets can become misaligned during long term acquisition, so someone should be on standby to fix them in between timepoints, without moving the specimen, thus adoption of adaptive light sheet technologies is a necessity (Royer *et al.*, 2016).

Ending this thesis I would like to discuss about tracking and the future of it. Tracking is very time consuming, for example the fully tracked embryo of 350 timepoints, took 4 months to be tracked and there is still work to do on it. To produce a quality work on the development of the embryo, it is needed to track multiple embryos to produce statistics, which are going to take months or even years of tracking. New

advancements in Artificial Intelligence, hopefully, are focusing on making it fully automatic. Elephant (Sugawara, Çevrim and Averof, 2022) is one such algorithm, based on Mastodon framework, segmentation is done by using a pretrained U-net, a convolutional neural network (CNN), if the pretrained model performs poorly it can be retrained with only sparse annotation.

As the last part of this discussion part and this thesis, I would like to put emphasis on the future directions of this project. The next step of this project is to study the lineage of an embryo with one ectoderm cell ablated and see how the regulation in such an embryo will work to still produce a capable adult. Similar work has been done by (Alwes, Hitchen and Extavour, 2011). During this study it was shown that the division patterns become irregular and the egg will try to cover the empty space produced by the ablation with daughters of other micromeres, without changing the different stages of gastrulation and migration. To enhance this study I consider 2 important actions: comparison with other similar organisms like *O. Cavimana* and the application of new technological advancements to enhance analysis or make resolution on even deeper parts of the embryo better.

5. Bibliography:

- (PDF) *Molecular Signalling Mechanisms at the μ -Opioid Receptor* (no date). Available at: https://www.researchgate.net/publication/339297870_Molecular_Signalling_Mechanisms_at_the_-Opioid_Receptor (Accessed: 4 August 2022).
- Abdollahpour, D. *et al.* (2010) ‘Spatiotemporal Airy light bullets in the linear and nonlinear regimes’, *Physical Review Letters*, 105(25). Available at: <https://doi.org/10.1103/PHYSREVLTT.105.253901>.
- Agard, D.A. (2003) ‘Optical Sectioning Microscopy: Cellular Architecture in Three Dimensions’, <http://dx.doi.org/10.1146/annurev.bb.13.060184.001203>, 13, pp. 191–219. Available at: <https://doi.org/10.1146/ANNUREV.BB.13.060184.001203>.
- Alwes, F., Hinchey, B. and Extavour, C.G. (2011) ‘Patterns of cell lineage, movement, and migration from germ layer specification to gastrulation in the amphipod crustacean *Parhyale hawaiiensis*’, *Developmental biology*, 359(1), pp. 110–123. Available at: <https://doi.org/10.1016/J.YDBIO.2011.07.029>.
- Amat, F. *et al.* (2015) ‘Efficient processing and analysis of large-scale light-sheet microscopy data’, *Nature Protocols*, 10(11), pp. 1679–1696. Available at: <https://doi.org/10.1038/NPROT.2015.111>.
- Besl, P.J. and McKay, N.D. (1992) ‘A Method for Registration of 3-D Shapes’, *IEEE Transactions on Pattern Analysis and Machine Intelligence*, 14(2), pp. 239–256. Available at: <https://doi.org/10.1109/34.121791>.
- Browne, W.E. *et al.* (2005) ‘Stages of embryonic development in the amphipod crustacean, *Parhyale hawaiiensis*’, *genesis*, 42(3), pp. 124–149. Available at: <https://doi.org/10.1002/gene.20145>.
- Buckingham, M.E. and Meilhac, S.M. (2011) ‘Tracing cells for tracking cell lineage and clonal behavior’, *Developmental cell*, 21(3), pp. 394–409. Available at: <https://doi.org/10.1016/J.DEVCEL.2011.07.019>.
- Chhetri, R.K. *et al.* (2015) ‘Whole-animal functional and developmental imaging with isotropic spatial resolution’, *Nature Methods*, 12(12), pp. 1171–1178. Available at: <https://doi.org/10.1038/nmeth.3632>.
- Chong, A. *et al.* (2010) ‘Airy-Bessel wave packets as versatile linear light bullets’, *Nature Photonics*, 4(2), pp. 103–106. Available at: <https://doi.org/10.1038/NPHOTON.2009.264>.
- Confocal Microscopy | Principle & Applications | ibidi* (no date). Available at: <https://ibidi.com/content/216-confocal-microscopy> (Accessed: 4 August 2022).
- Edelstein, A.D. *et al.* (2014) ‘Advanced methods of microscope control using μ Manager software’, *Journal of Biological Methods*, 1(2), p. e10. Available at: <https://doi.org/10.14440/jbm.2014.36>.
- Foley, J.D., Fischler, M.A. and Bolles, R.C. (1981) ‘Graphics and Image Processing Random Sample Consensus: A Paradigm for Model Fitting with Applications to Image Analysis and Automated Cartography’.
- Gerberding, M., Browne, W.E. and Patel, N.H. (2002) ‘Cell lineage analysis of the amphipod crustacean *Parhyale hawaiiensis* reveals an early restriction of cell fates’, *Development*, 129(24), pp. 5789–5801. Available at: <https://doi.org/10.1242/dev.00155>.
- Gilchrist, J. (no date) ‘PARALLEL DATA COMPRESSION WITH BZIP2’.
- Girstmair, J. *et al.* (2022) ‘Time to Upgrade: A New OpenSPIM Guide to Build and Operate Advanced OpenSPIM Configurations’, *Advanced Biology*, 6(4). Available at: <https://doi.org/10.1002/adbi.202101182>.
- GitHub - mastodon-sc/mastodon: Mastodon – a large-scale tracking and track-editing framework for large, multi-view images.* (no date). Available at: <https://github.com/mastodon-sc/mastodon> (Accessed: 17 August 2022).
- Goshtasby, A.A. (2005) ‘Fusion of multi-exposure images’, *Image and Vision Computing*, 23(6), pp. 611–618. Available at: <https://doi.org/10.1016/J.IMAVIS.2005.02.004>.
- Hörl, D. *et al.* (2018) ‘BigStitcher: Reconstructing high-resolution image datasets of cleared and expanded samples’, *bioRxiv*, p. 343954. Available at: <https://doi.org/10.1101/343954>.

- Huisken, J. *et al.* (2004) ‘Optical sectioning deep inside live embryos by selective plane illumination microscopy’, *Science*, 305(5686), pp. 1007–1009. Available at: <https://doi.org/10.1126/science.1100035>.
- Jaqaman, K. *et al.* (2008) ‘Robust single-particle tracking in live-cell time-lapse sequences’, *Nature Methods*, 5(8), pp. 695–702. Available at: <https://doi.org/10.1038/nmeth.1237>.
- Konstantinides, N. and Averof, M. (2014) ‘A common cellular basis for muscle regeneration in arthropods and vertebrates’, *Science*, 343(6172), pp. 788–791. Available at: <https://doi.org/10.1126/SCIENCE.1243529>.
- Kontarakis, Z. and Pavlopoulos, A. (2014) ‘Transgenesis in non-model organisms: The case of parhyale’, *Methods in Molecular Biology*, 1196, pp. 145–181. Available at: https://doi.org/10.1007/978-1-4939-1242-1_10.
- Koranne, S. (2011) ‘Hierarchical Data Format 5 : HDF5’, *Handbook of Open Source Tools*, pp. 191–200. Available at: https://doi.org/10.1007/978-1-4419-7719-9_10.
- Kretschmar, K. and Watt, F.M. (2012) ‘Leading Edge Primer Lineage Tracing’, *Cell*, 148, pp. 33–45. Available at: <https://doi.org/10.1016/j.cell.2012.01.002>.
- Lucy, L.B. (1974) ‘An iterative technique for the rectification of observed distributions’, 79(6).
- McDole, K. *et al.* (2018) ‘In Toto Imaging and Reconstruction of Post-Implantation Mouse Development at the Single-Cell Level’, *Cell*, 175(3), pp. 859–876.e33. Available at: <https://doi.org/10.1016/J.CELL.2018.09.031>.
- Meinert, T. and Rohrbach, A. (2019) ‘Light-sheet microscopy with length-adaptive Bessel beams’, *Biomedical Optics Express*, 10(2), p. 670. Available at: <https://doi.org/10.1364/boe.10.000670>.
- Nast, A.R. and Extavour, C.G. (2014) ‘Ablation of a single cell from eight-cell embryos of the amphipod crustacean *Parhyale hawaiiensis*’, *Journal of visualized experiments : JoVE* [Preprint], (85). Available at: <https://doi.org/10.3791/51073>.
- Olarte, O.E. *et al.* (2018) ‘Light-sheet microscopy: a tutorial’, *Advances in Optics and Photonics*, 10(1), p. 111. Available at: <https://doi.org/10.1364/aop.10.000111>.
- Phalloidin staining protocol | Abcam* (no date). Available at: <https://www.abcam.com/protocols/phalloidin-staining-protocol> (Accessed: 11 August 2022).
- Preibisch, S. *et al.* (2010) ‘Software for bead-based registration of selective plane illumination microscopy data’, *Nature Methods*, 7(6), pp. 418–419. Available at: <https://doi.org/10.1038/NMETH0610-418>.
- Remington, S.J. (2011) ‘Green fluorescent protein: A perspective’. Available at: <https://doi.org/10.1002/pro.684>.
- Richardson, W.H. (1972) ‘Bayesian-Based Iterative Method of Image Restoration*’, *JOSA, Vol. 62, Issue 1*, pp. 55–59, 62(1), pp. 55–59. Available at: <https://doi.org/10.1364/JOSA.62.000055>.
- Royer, L.A. *et al.* (2016) ‘Adaptive light-sheet microscopy for long-term, high-resolution imaging in living organisms’, *Nature Biotechnology*, 34(12), pp. 1267–1278. Available at: <https://doi.org/10.1038/nbt.3708>.
- Santi, P.A. (2011) ‘Light sheet fluorescence microscopy: a review’, *The journal of histochemistry and cytochemistry : official journal of the Histochemistry Society*, 59(2), pp. 129–138. Available at: <https://doi.org/10.1369/0022155410394857>.
- Scholtz, G. and Wolff, C. (2002) ‘Cleavage, gastrulation, and germ disc formation of the amphipod *Orchestia cavimana* (Crustacea, Malacostraca, Peracarida)’, *Contributions to Zoology*, 71(1–3), pp. 9–28. Available at: <https://doi.org/10.1163/18759866-0710103002>.
- Serra, J. (1986) ‘Introduction to mathematical morphology’, *Computer Vision, Graphics, and Image Processing*, 35(3), pp. 283–305. Available at: [https://doi.org/10.1016/0734-189X\(86\)90002-2](https://doi.org/10.1016/0734-189X(86)90002-2).
- Shimomura, O. (1979) ‘Structure of the chromophore of *Aequorea* green fluorescent protein’, *FEBS Letters*, 104(2), pp. 220–222. Available at: [https://doi.org/10.1016/0014-5793\(79\)80818-2](https://doi.org/10.1016/0014-5793(79)80818-2).
- Skraba, P. *et al.* (2010) ‘Persistence-based segmentation of deformable shapes’, *undefined*, pp. 45–52. Available at:

<https://doi.org/10.1109/CVPRW.2010.5543285>.

Stamatakis, E. and Pavlopoulos, A. (2016) 'Non-insect crustacean models in developmental genetics including an encomium to *Parhyale hawaiiensis*', *Current Opinion in Genetics & Development*, 39, pp. 149–156. Available at: <https://doi.org/10.1016/J.GDE.2016.07.004>.

Stelzer, E.H.K. (2014) 'Light-sheet fluorescence microscopy for quantitative biology', *Nature Methods* 2014 12:1, 12(1), pp. 23–26. Available at: <https://doi.org/10.1038/nmeth.3219>.

Stelzer, E.H.K. *et al.* (2021) 'Light sheet fluorescence microscopy', *Nature Reviews Methods Primers* 2021 1:1, 1(1), pp. 1–25. Available at: <https://doi.org/10.1038/s43586-021-00069-4>.

Sugawara, K., Çevrim, Ç. and Averof, M. (2022) 'Tracking cell lineages in 3D by incremental deep learning', *eLife*, 11. Available at: <https://doi.org/10.7554/eLife.69380>.

Sulston, J.E. *et al.* (1983) 'The embryonic cell lineage of the nematode *Caenorhabditis elegans*', *Developmental Biology*. Academic Press, pp. 64–119. Available at: [https://doi.org/10.1016/0012-1606\(83\)90201-4](https://doi.org/10.1016/0012-1606(83)90201-4).

Sun, D.A. and Patel, N.H. (2019) 'The amphipod crustacean *Parhyale hawaiiensis*: An emerging comparative model of arthropod development, evolution, and regeneration', *WIREs Developmental Biology*, 8(5), p. e355. Available at: <https://doi.org/10.1002/wdev.355>.

Tinevez, J.Y. *et al.* (2017) 'TrackMate: An open and extensible platform for single-particle tracking', *Methods*, 115, pp. 80–90. Available at: <https://doi.org/10.1016/J.YMETH.2016.09.016>.

Tomer, R. *et al.* (2012) 'Quantitative high-speed imaging of entire developing embryos with simultaneous multiview light-sheet microscopy', *Nature Methods*, 9(7), pp. 755–763. Available at: <https://doi.org/10.1038/nmeth.2062>.

Verveer, P.J. and Jovin, T.M. (1998) 'Improved restoration from multiple images of a single object: application to fluorescence microscopy', *Applied Optics*, Vol. 37, Issue 26, pp. 6240–6246, 37(26), pp. 6240–6246. Available at: <https://doi.org/10.1364/AO.37.006240>.

Vettenburg, T. *et al.* (2014) 'Light-sheet microscopy using an Airy beam', *Nature Methods*, 11(5), pp. 541–544. Available at: <https://doi.org/10.1038/nmeth.2922>.

VOIE, A.H., BURNS, D.H. and SPELMAN, F.A. (1993) 'Orthogonal-plane fluorescence optical sectioning: Three-dimensional imaging of macroscopic biological specimens', *Journal of Microscopy*, 170(3), pp. 229–236. Available at: <https://doi.org/10.1111/j.1365-2818.1993.tb03346.x>.

Wan, Y., McDole, K. and Keller, P.J. (2019) 'Light-Sheet Microscopy and Its Potential for Understanding Developmental Processes', <https://doi.org/10.1146/annurev-cellbio-100818-125311>, 35, pp. 655–681. Available at: <https://doi.org/10.1146/ANNUREV-CELLBIO-100818-125311>.

Widefield Fluorescence Microscopy | Principle & Applications | ibidi (no date). Available at: <https://ibidi.com/content/215-widefield-fluorescence> (Accessed: 4 August 2022).

Wolff, C. *et al.* (2018) 'Multi-view light-sheet imaging and tracking with the MaMuT software reveals the cell lineage of a direct developing arthropod limb', *eLife*, 7. Available at: <https://doi.org/10.7554/ELIFE.34410>.

Wolff, C. and Scholtz, G. (2006) 'Cell lineage analysis of the mandibular segment of the amphipod *Orchestia cavimana* reveals that the crustacean paragnaths are sternal outgrowths and not limbs', *Frontiers in Zoology*, 3(1), p. 19. Available at: <https://doi.org/10.1186/1742-9994-3-19>.

Yakupova, E.I. *et al.* (2019) 'Congo Red and amyloids: History and relationship', *Bioscience Reports*. Portland Press Ltd. Available at: <https://doi.org/10.1042/BSR20181415>.